Received: 5 January 2022 | Accepted: 7 March 2022

DOI: 10.1002/nme.6964

RESEARCH ARTICLE

WILEY

An adaptive projection-based model reduction method for nonlinear mechanics with internal variables: Application to thermo-hydro-mechanical systems

Angelo Iollo[1,2] | **Giulia Sambataro**[1,2] | **Tommaso Taddei**[1,2]

[1]IMB, UMR 5251, Univ. Bordeaux, Talence, France

[2]INRIA, Inria Bordeaux Sud-Ouest, Team MEMPHIS, Talence, France

Correspondence
Giulia Sambataro, INRIA, Inria Bordeaux Sud-Ouest, Team MEMPHIS, 33400 Talence, France.
Email: giulia.sambataro@inria.fr

Funding information
Andra (National Agency for Radioactive Waste Management); European Union's Horizon 2020 Research and Innovation Programme, Grant/Award Number: 872442

Abstract

We propose a projection-based monolithic model order reduction procedure for a class of problems in nonlinear mechanics with internal variables. The work is motivated by applications to thermo-hydro-mechanical (THM) systems for radioactive waste disposal. THM equations model the behavior of temperature, pore water pressure, and solid displacement in the neighborhood of geological repositories, which contain radioactive waste and are responsible for a significant thermal flux toward the Earth's surface. We develop an adaptive sampling strategy based on the POD-Greedy method, and we develop an element-wise empirical quadrature hyper-reduction procedure to reduce assembling costs. We present numerical results for a two-dimensional THM system to illustrate and validate the proposed methodology.

KEYWORDS

model order reduction, nonlinear mechanics, parameterized partial differential equations

1 | INTRODUCTION

1.1 | Model reduction for a class of models in nonlinear mechanics

The disposal and storage of high-level radioactive waste materials in geological means require a careful assessment of the long-term effects on neighboring areas. The system behavior is well described by time-dependent large-scales coupled systems of partial differential equations (PDEs), which take into account the thermal, hydraulic, and mechanical response of the geological medium. Numerical simulation of these systems is challenging due to several difficulties: first, finite element (FE) models of the problem are highly nonlinear, time-dependent, and high-dimensional; second, due to the uncertainty in model parameters, we need to solve the model for many different system configurations (*many-query* problem). In this work, we shall devise a model order reduction (MOR) strategy to speed up parametric studies for radioactive waste disposal applications.

In this contribution, we study a general class of nonlinear problems in structural mechanics with internal variables. We consider the spatial variable x in the Lipschitz domain $\Omega \subset \mathbb{R}^d$ with $d = 2, 3$, and the time variable t in the time internal $(0, T_f)$, where T_f is the final time. We further define the vector of parameters μ in the compact parameter region $\mathcal{P} \subset \mathbb{R}^P$. We introduce the state (or primary) variables $\underline{U}$ and internal (or dependent) variables $\underline{W}$; we denote by $\mathcal{X}$ and $\mathcal{W}$ suitable Hilbert spaces in Ω for $\underline{U}$ and $\underline{W}$, and we define the space of continuous functions from $(0, T_f)$ to $\mathcal{X}$ and $\mathcal{W}$, $C(0, T_f; \mathcal{X})$ and $C(0, T_f; \mathcal{W})$. Then, we introduce the parameterized problem of interest: given $\mu \in \mathcal{P}$, find $(\underline{U}_\mu, \underline{W}_\mu) \in$

$C(0, T_f; \mathcal{X}) \times C(0, T_f; \mathcal{W})$ such that

$$\begin{cases} \mathcal{G}_\mu(\underline{U}_\mu, \partial_t \underline{U}_\mu, \underline{W}_\mu) = 0, & \text{in } \Omega \times (0, T_f), \\ \dot{\underline{W}}_\mu = \mathcal{F}_\mu(\underline{U}_\mu, \underline{W}_\mu), & \text{in } \Omega \times (0, T_f), \end{cases} \tag{1}$$

with suitable initial and boundary conditions. Here, $\mathcal{G}_\mu$ is a nonlinear second-order in space, first-order in time differential operator that is associated with the equilibrium equations, while $\mathcal{F}_\mu$ is a set of ordinary differential equations (ODEs) that is associated with the constitutive laws.

Our methodology is motivated by the application to thermo-hydro-mechanical (THM) systems of the form (1), which are widely used to model the system's response for radioactive waste disposal applications. Radioactive material is placed in an array of horizontal boreholes (dubbed *alveoli*) deep underground: due to the large temperature of the alveoli, a thermal flux is generated; the thermal flux then drives the mechanical and hydraulic response of the medium over the course of several years. We refer to Section 4 for a detailed discussion of the considered THM model and boundary conditions.

1.2 | Objective of the work and relationship to previous works

We propose a projection-based monolithic MOR[1-3] technique for problems of the form (1), with particular emphasis on THM systems. The approach is characterized by an offline/online splitting to reduce the marginal cost, and relies on Galerkin projection to devise a reduced-order model (ROM) for the solution coefficients. We rely on hyper-reduction to speed up the assembly of the ROM during the online stage, and we rely on adaptive sampling to reduce the offline training costs.

The contribution of this work is the development of a POD-Greedy technique for coupled problems with internal variables. First, we present a time-average a posteriori error indicator and compare it with a more standard discrete $L^2(0, T_f; \mathcal{X}')$ dual residual in terms of computational and memory costs and effectivity. This is crucial for the efficiency of the adaptive method. Second, we apply a greedy sampling (based on the proposed error indicator) to effectively explore the parameter domain. Third, we introduce in this framework a hyper-reduction technique based on an element-wise empirical quadrature (EQ) procedure.

EQ procedures also dubbed mesh sampling and weighting have been first proposed in References 4-6 and further developed in several other works including Reference 7: the key feature of EQ is to recast the problem of hyper-reduction as a sparse representation problem and then resort to state-of-the-art techniques in machine learning and signal processing to estimate the solution to the resulting optimization problem. Here, we rely on the approach employed in Reference 8, which combines the methods in References 4 and 5 and relies on non-negative least-squares to estimate the solution to the sparse representation problem.

As discussed in Section 3, the presence of internal variables requires several changes to the EQ approach in Reference 8. Our approach relies on a different treatment of primary and internal variables compared to the works in Reference 9 and 10, as explained in Section 3.2. In addition, in the present work we aim at solving coupled systems that model the interaction between mechanic, thermal and hydraulic response, as described in Section 4. In Section 3, we clarify to what extent the management of internal variables requires a careful adaptation of the MOR technique illustrated in Reference 8 and we briefly compare our treatment of internal variables with References 9 and 10.

We emphasize that several other hyper-reduction techniques have been proposed in the literature including the empirical interpolation method (EIM[11]) and its discrete variant,[12] the approach in Reference 13, and Gappy-POD.[14,15] We also refer to References 16 and 17 for further empirical (or reduced) quadrature procedures for problems in nonlinear mechanics. A thorough comparison of state-of-the-art hyper-reduction techniques is beyond the scope of this work.

The POD-Greedy algorithm was introduced in Reference 18 and analyzed in Reference 19: the approach combines proper orthogonal decomposition (POD[20-22]) to compress temporal trajectories with a greedy search driven by an error indicator to explore the parameter domain. In this work, similar to Reference 23, we rely on a time-averaged error indicator to drive the greedy search; furthermore, we test two different compression strategies to update the POD basis at each greedy iteration.

We further observe that the development of online-efficient adaptive ROMs for problems of the form (1) is extremely limited in the literature. Relevant examples include the works in References 13, 24, and 25, which, however, do not

consider adaptive sampling. As regards the application of MOR to THM systems, we recall the recent contribution by Larion et al.:[26] note, however, that the work in Reference 26 deals with a linearized THM model without internal variables.

1.3 | Outline

The outline of this article is the following. In Section 2, we briefly present the mathematical model and the numerical discretization for the general class of nonlinear problems in structural mechanics defined in (1). In Section 3, we present the MOR technique: to simplify the presentation, we first discuss the solution reproduction problem and then we extend the approach to the parametric case. Section 4 contains details of the THM mathematical model considered in the numerical section. In Section 5, we present extensive numerical investigations for a two-dimensional THM system. In Section 6, we draw some conclusions and we outline a number of subjects of ongoing research.

2 | FORMULATION

2.1 | Notation

In this section, we omit dependence on the parameter. Given $\Omega \subset \mathbb{R}^d$, we define the triangulation $\{\mathtt{D}_k\}_{k=1}^{N_\mathrm{e}}$, where N_e denotes the total number of elements, the nodes $\{x_j^{\mathrm{hf}}\}_{j=1}^{\mathcal{N}}$ and the connectivity matrix $\mathtt{T} \in \mathbb{N}^{N_\mathrm{e},n_\mathrm{lp}}$ such that $\mathtt{T}_{k,i} \in \{1, \dots, \mathcal{N}\}$ is the index of the ith node of the kth element of the mesh and n_lp is the number of degrees of freedom in each element. We remark that throughout the article the acronym HF stands for high-fidelity discretization.

Then, we introduce the continuous Lagrangian FE basis $\{\varphi_i\}_{i=1}^{\mathcal{N}}$ associated with the triangulation $\{\mathtt{D}_k\}_{k=1}^{N_\mathrm{e}}$, such that $\varphi_i(x_j^{\mathrm{hf}}) = \delta_{i,j}$, and we introduce the FE space for the state variables:

$$\mathcal{X}_{\mathrm{hf}} := \mathrm{span}\left\{ \varphi_i \underline{e}_j : \quad i = 1, \dots, \mathcal{N}, \ \ j = 1, \dots, D_{\mathrm{eq}} \right\}, \tag{2}$$

where $\underline{e}_1, \dots, \underline{e}_{D_{\mathrm{eq}}}$ are the elements of the canonical basis and D_{eq} is the number of state variables.

We define the state variables for the specific problem of interest in Section 4.1.

We denote by $\|\cdot\| = \sqrt{(\cdot,\cdot)}$ the norm of $\mathcal{X}_{\mathrm{hf}}$; furthermore, given $\underline{u} \in \mathcal{X}_{\mathrm{hf}}$, we denote by $\underline{\mathbf{u}} \in \mathbb{R}^{\mathcal{N},D_{\mathrm{eq}}}$ the corresponding vector (or matrix) of coefficients such that $(\underline{\mathbf{u}})_{j,\ell} = \left(\underline{u}(x_j^{\mathrm{hf}})\right)_\ell$ for $j = 1, \dots, \mathcal{N}$ and $\ell = 1, \dots, D_{\mathrm{eq}}$; notation $\underline{\mathbf{u}}(:,\ell)$ refers to the ℓth column of the matrix $\underline{\mathbf{u}}$.

In view of the MOR formulation, we introduce the elemental restriction operators $\mathbf{E}_k : \mathbb{R}^{\mathcal{N}} \to \mathbb{R}^{n_\mathrm{lp}}$ such that

$$\left(\mathbf{E}_k \underline{\mathbf{u}}\right)_{i,\ell} = \left(\underline{u}(x_{\mathtt{T}_{k,i}}^{\mathrm{hf}})\right)_\ell, \quad i = 1, \dots, n_\mathrm{lp}, \ \ell = 1, \dots, D_{\mathrm{eq}}, \ k = 1, \dots, N_\mathrm{e}. \tag{3a}$$

Furthermore, we introduce the quadrature points $\{x_{q,k}^{\mathrm{hf,q}}\}_{q,k} \subset \Omega$, such that $x_{q,k}^{\mathrm{hf,q}}$ is the qth quadrature point of the kth element of the mesh, with $q = 1, \dots, n_\mathrm{q}$, and the operators $\mathbf{E}_k^{\mathrm{qd}} : \mathbb{R}^{\mathcal{N}} \to \mathbb{R}^{n_\mathrm{q}}$ and $\mathbf{E}_k^{\mathrm{qd},\nabla} : \mathbb{R}^{\mathcal{N}} \to \mathbb{R}^{n_\mathrm{q},d}$ such that

$$\left(\mathbf{E}_k^{\mathrm{qd}} \underline{\mathbf{u}}\right)_{q,\ell} = \left(\underline{u}(x_{q,k}^{\mathrm{hf,q}})\right)_\ell, \quad \left(\mathbf{E}_k^{\mathrm{qd},\nabla} \underline{\mathbf{u}}\right)_{q,\ell,j} = \left(\frac{\partial}{\partial x_j}\underline{u}(x_{q,k}^{\mathrm{hf,q}})\right)_\ell, \tag{3b}$$

where $q = 1, \dots, n_\mathrm{q}$, $\ell = 1, \dots, D_{\mathrm{eq}}$, $k = 1, \dots, N_\mathrm{e}$, and $j = 1, \dots, d$. To shorten notation, in the following, we further define $\mathbf{E}_k^{\mathrm{qd},\star} : \mathbb{R}^{\mathcal{N}} \to \mathbb{R}^{n_\mathrm{q},d+1}$ such that

$$\left(\mathbf{E}_k^{\mathrm{qd},\star} \underline{\mathbf{u}}\right)_{q,\ell,1} = \left(\mathbf{E}_k^{\mathrm{qd}} \underline{\mathbf{u}}\right)_{q,\ell}, \quad \left(\mathbf{E}_k^{\mathrm{qd},\star} \underline{\mathbf{u}}\right)_{q,\ell,2\dots,d+1} = \left(\mathbf{E}_k^{\mathrm{qd},\nabla} \underline{\mathbf{u}}\right)_{q,\ell,\cdot}. \tag{3c}$$

Remark 1. For the THM problem considered in this work, the state $\underline{U}$ contains the displacement $\underline{u}$, the water pressure p, and the temperature T ($D_{\mathrm{eq}} = 2 + d$); as discussed in Reference 27, to avoid instabilities, it is important to use polynomials of degree κ for displacement and $\kappa - 1$ for pressure and temperature: as a result, we should introduce separate restriction operators and separate FE spaces for the different components of the state. In the main body of the article, we

choose to not explicitly address this issue to simplify notation: we remark that the extension to κ-($\kappa-1$) discretizations is computationally tedious but methodologically straightforward.

2.2 | FE discretization of (1)

We introduce the time grid $0 = t^{(0)} < t^{(1)} < \cdots < t^{(J_{\max})} = T_{\mathrm{f}}$ such that $t^{(j)} = j\Delta t$. We denote by $\{\underline{U}_{\mathrm{hf}}^{(j)}\}_{j=1}^{J_{\max}} \subset \mathcal{X}_{\mathrm{hf}}$ the FE approximation of the state variables at all times, that is, the ℓth column of $\underline{U}_{\mathrm{hf}}^{(j)}$ is the approximation of the ℓth state variable at time $t^{(j)}$. On the other hand, we denote by $\underline{\mathbf{W}}_{\mathrm{hf}}^{(j)} \in \mathbb{R}^{n_{\mathrm{q}},N_{\mathrm{e}},D_{\mathrm{int}}}$ the tensor associated with the evaluation of the internal variables at time $t^{(j)}$ in the quadrature points:

$$\left(\underline{\mathbf{W}}_{\mathrm{hf}}^{(j)}\right)_{q,k,\ell} = \left(\underline{W}_{\mathrm{hf}}^{(j)}(x_{q,k}^{\mathrm{hf,q}})\right)_{\ell}, \quad q = 1, \ldots, n_{\mathrm{q}},\ k = 1, \ldots, N_{\mathrm{e}},\ \ell = 1, \ldots, D_{\mathrm{int}}.$$

Given $\ell \in \{1, \ldots, D_{\mathrm{eq}}\}$, we further denote by $\mathtt{I}_{\mathrm{dir}}^{\ell} \subset \{1, \ldots, N_{\mathrm{hf}}\}$ the indices associated with Dirichlet boundary conditions (if any) of the ℓth state component, and we denote by $\underline{\mathbf{g}}_{\mathrm{dir},\ell}^{(j)} \in \mathbb{R}^{|\mathtt{I}_{\mathrm{dir}}^{\ell}|}$ the vector that contains the value of the ℓth state component at each Dirichlet node at time $t^{(j)}$.

We state the FE discretization of (1) as follows: for $j = 1, 2, \ldots$, find $(\underline{U}_{\mathrm{hf}}^{(j)}, \underline{W}_{\mathrm{hf}}^{(j)})$ such that

$$\begin{cases} \mathcal{R}^{\mathrm{hf}}\left(\underline{\mathbf{U}}_{\mathrm{hf}}^{(j)}, \underline{\mathbf{U}}_{\mathrm{hf}}^{(j-1)}, \underline{\mathbf{W}}_{\mathrm{hf}}^{(j)}, \underline{\mathbf{W}}_{\mathrm{hf}}^{(j-1)}, \underline{\mathbf{V}}\right) = 0, \ \ \forall\, \underline{V} \in \mathcal{X}_{\mathrm{hf},0}; \\ \underline{\mathbf{U}}_{\mathrm{hf}}^{(j)}(\mathtt{I}_{\mathrm{dir}}^{\ell}, \ell) = \underline{\mathbf{g}}_{\mathrm{dir},\ell}^{(j)}, \quad \ell = 1, \ldots, D_{\mathrm{eq}}; \\ \left(\underline{\mathbf{W}}_{\mathrm{hf}}^{(j)}\right)_{q,k,\ell} = \mathcal{F}_{\ell}^{\mathrm{hf}}\left(\left(\mathbf{E}_k^{\mathrm{qd},\star}\underline{\mathbf{U}}_{\mathrm{hf}}^{(j)}\right)_{q,\cdot}, \ \left(\mathbf{E}_k^{\mathrm{qd},\star}\underline{\mathbf{U}}_{\mathrm{hf}}^{(j-1)}\right)_{q,\cdot}, \ \left(\underline{\mathbf{W}}_{\mathrm{hf}}^{(j-1)}\right)_{q,k,\cdot}\right), \\ \qquad\qquad q = 1, \ldots, n_{\mathrm{q}}, k = 1, \ldots, N_{\mathrm{e}}, \ell = 1, \ldots, D_{\mathrm{int}}, \end{cases} \tag{4}$$

where $\mathcal{X}_{\mathrm{hf},0} := \{\underline{V} \in \mathcal{X}_{\mathrm{hf}} \ : \ \underline{\mathbf{V}}(\mathtt{I}_{\mathrm{dir}}^{\ell}, \ell) = 0, \ell = 1, \ldots, D_{\mathrm{eq}}\}$ is the test space for all state equations. Note that $\mathcal{R}^{\mathrm{hf}}$ and $\underline{\mathcal{F}}^{\mathrm{hf}}$ are the discrete counterparts of the operators $\mathcal{G}$ and $\underline{\mathcal{F}}$ in (1). Note also that the constitutive laws are stated in the quadrature points of the mesh and the internal fields should be computed in the quadrature points of the mesh. Dirichlet boundary conditions are imposed via a lifting; Neumann boundary conditions are introduced in the weak formulation associated to the first equation in system (4) via the Green's formula. We refer to Section 4 for the particular form of problem (4) associated to THM systems.

The underlying problem is second-order in space and first-order in time. At each time step, following Reference 27, we solve (4) for $\underline{U}_{\mathrm{hf}}^{(j)}$ using a Newton method with line search; the method requires the computation of the Jacobian and the solution to a coupled linear system of size $\mathcal{N} \cdot D_{\mathrm{eq}}$.

In view of the introduction of the MOR methodology, in particular the hyper-reduction procedure, we write the residual $\mathcal{R}^{\mathrm{hf}}$ as the sum of local contributions.

$$\begin{aligned} &\mathcal{R}^{\mathrm{hf}}\left(\underline{\mathbf{U}}^{(j)}, \underline{\mathbf{U}}^{(j-1)}, \underline{\mathbf{W}}^{(j)}, \underline{\mathbf{W}}^{(j-1)}, \underline{\mathbf{V}}\right) = \\ &\sum_{k=1}^{N_{\mathrm{e}}} r_k^{\mathrm{hf}}\left(\mathbf{E}_k\underline{\mathbf{U}}^{(j)}, \ \mathbf{E}_k\underline{\mathbf{U}}^{(j-1)}, \ \left(\underline{\mathbf{W}}^{(j)}\right)_{\cdot,k,\cdot}, \ \left(\underline{\mathbf{W}}^{(j-1)}\right)_{\cdot,k,\cdot}, \ \mathbf{E}_k\underline{\mathbf{V}}^{(j)}\right). \end{aligned} \tag{5}$$

As explained in Section 3, this decomposition provides the foundation of our hyper-reduction procedure.

3 | METHODOLOGY

We propose a time-marching Galerkin ROM based on linear approximations. More precisely, we consider approximations of the form

$$\widehat{\underline{U}}_{\mu}^{(j)} = \underline{Z}\,\widehat{\boldsymbol{\alpha}}_{\mu}^{(j)} = \sum_{n=1}^{N}\left(\widehat{\boldsymbol{\alpha}}_{\mu}^{(j)}\right)_n \underline{\zeta}_n, \quad j = 1, \ldots, J_{\max}, \tag{6}$$

where $\{\widehat{\boldsymbol{\alpha}}_\mu^{(j)}\}_{j=1}^{J_{\max}} \subset \mathbb{R}^N$ are referred to as solution coefficients and are computed by solving a suitable ROM, while $\underline{Z} : \mathbb{R}^N \to \mathcal{X}_{\mathrm{hf}}$ is the reduced-order basis (ROB) and $\mathcal{Z} := \mathrm{span}\{\underline{\zeta}_n\}_{n=1}^N$ is the reduced space. In presence of nonhomogeneous Dirichlet conditions, it is convenient to consider affine approximations of the form $\underline{\widehat{U}}_\mu^{(j)} = \underline{H}\mathbf{g}^{(j)} + \underline{Z}\,\widehat{\boldsymbol{\alpha}}_\mu^{(j)}$, where $\underline{H}$ is a suitable lifting operator (see, e.g., Reference 8) and $\mathcal{Z} \subset \mathcal{X}_{\mathrm{hf},0}$: since in this work, we consider homogeneous Dirichlet conditions, we do not address the treatment of nonhomogeneous conditions. We consider a single reduced basis $\underline{Z}$ for all state variables in $\{\underline{U}_{\mathrm{hf}}^{(j)}\}_{j=1}^{J_{\max}}$; we discuss the choice of the inner product in Section 4 (cf. Equation 33).

The Galerkin ROM is obtained by projecting (4) onto the reduced space $\mathcal{Z}$: this leads to a nonlinear system of N equations at each time step. To reduce assembly costs, it is important to avoid integration over the whole integration domain. Toward this end, we define the indices associated with the "sampled elements" $\mathtt{I}_{\mathrm{eq}} \subset \{1, \dots, N_{\mathrm{e}}\}$ and we define the EQ residual:

$$\begin{aligned}&\mathcal{R}_\mu^{\mathrm{eq}}\left(\underline{\mathbf{U}}^{(j)}, \underline{\mathbf{U}}^{(j-1)}, \underline{\mathbf{W}}^{(j)}, \underline{\mathbf{W}}^{(j-1)}, \underline{\mathbf{V}}\right) = \\ &\sum_{k \in \mathtt{I}_{\mathrm{eq}}} \rho_k^{\mathrm{eq}}\, r_{\mu,k}^{\mathrm{hf}}\left(\mathbf{E}_k\underline{\mathbf{U}}^{(j)}, \mathbf{E}_k\underline{\mathbf{U}}^{(j-1)}, \left(\underline{\mathbf{W}}^{(j)}\right)_{\cdot,k,\cdot}, \left(\underline{\mathbf{W}}^{(j-1)}\right)_{\cdot,k,\cdot}, \mathbf{E}_k\underline{\mathbf{V}}^{(j)}\right),\end{aligned} \tag{7a}$$

where $\boldsymbol{\rho}^{\mathrm{eq}} = [\rho_1^{\mathrm{eq}}, \dots, \rho_{N_{\mathrm{e}}}^{\mathrm{eq}}]^T$ is a sparse vector of positive weights such that $\rho_k^{\mathrm{eq}} = 0$ if $k \notin \mathtt{I}_{\mathrm{eq}}$. In conclusion, the Galerkin ROM reads as follows: for $j = 1, 2, \dots$, find $(\underline{\widehat{U}}_\mu^{(j)}, \underline{\widehat{W}}_\mu^{(j)})$ such that

$$\begin{cases}\mathcal{R}_\mu^{\mathrm{eq}}\left(\underline{\widehat{\mathbf{U}}}_\mu^{(j)}, \underline{\widehat{\mathbf{U}}}_\mu^{(j-1)}, \underline{\widehat{\mathbf{W}}}_\mu^{(j)}, \underline{\widehat{\mathbf{W}}}_\mu^{(j-1)}, \underline{\mathbf{V}}\right) = 0, \quad \forall\, \underline{V} \in \mathcal{Z}; \\ \left(\underline{\widehat{\mathbf{W}}}_\mu^{(j)}\right)_{q,k,\ell} = \mathcal{F}_{\mu,\ell}^{\mathrm{hf}}\left(\left(\mathbf{E}_k^{\mathrm{qd},\star}\underline{\widehat{\mathbf{U}}}_\mu^{(j)}\right)_{q,\cdot}, \left(\mathbf{E}_k^{\mathrm{qd},\star}\underline{\widehat{\mathbf{U}}}_\mu^{(j-1)}\right)_{q,\cdot}, \left(\underline{\widehat{\mathbf{W}}}_\mu^{(j-1)}\right)_{q,k,\cdot}\right), \\ \qquad q = 1, \dots, n_{\mathrm{q}}, k \in \mathtt{I}_{\mathrm{eq}}, \ell = 1, \dots, D_{\mathrm{int}}.\end{cases} \tag{7b}$$

Note that the internal variables need to be computed only in the sampled elements. Furthermore, computation of (7b) only requires the storage of the ROB in the sampled elements, $\{\mathbf{E}_k\underline{\boldsymbol{\zeta}}_n : n = 1, \dots, N, k \in \mathtt{I}_{\mathrm{eq}}\}$: provided that $|\mathtt{I}_{\mathrm{eq}}| \ll N_{\mathrm{e}}$, this leads to significant savings in terms of online assembly costs and also in terms of online memory costs.

In the remainder of this section, we shall discuss the construction of the ROB $\underline{Z}$ (*data compression*), the empirical quadrature rule $\boldsymbol{\rho}^{\mathrm{eq}}$ (*hyper-reduction*) and also the error indicator. To simplify the presentation, in Section 3.1, we focus on the solution reproduction problem, while in Section 3.2, we discuss the extension to the parametric problem.

3.1 | Solution reproduction problem

The solution reproduction problem refers to the task of reproducing the results obtained for a fixed value of the parameter μ. Algorithm 1 summarizes the procedure: during the offline stage, we compute the HF solution to (6) for a given parameter and we store snapshots of the state variables at select time steps $\mathtt{I}_{\mathrm{s}} \subset \{1, \dots, J_{\max}\}$; then, we use this piece of information to build a ROM for the state; then, during the online stage, we query the ROM for the same value of the parameter considered in the offline stage.

Algorithm 1. Solution reproduction problem: offline/online decomposition

Offline stage:

1: compute $\{\underline{\mathbf{U}}_{\mathrm{hf},\cdot}^{(j)}\}_{j \in \mathtt{I}_{\mathrm{s}}}, \mathtt{I}_{\mathrm{s}} \subset \{1, \dots, J_{\max}\}$;

2: construct the ROB $\underline{Z}$; ▷ Section 3.1.1

3: construct the weights $\boldsymbol{\rho}^{\mathrm{eq}}$. ▷ Section 3.1.2

Online stage:

4: compute $\{\widehat{\boldsymbol{\alpha}}_\mu^{(j)}\}_{j=1}^{J_{\max}}$ by solving the ROM (7).

The solution reproduction problem is of little practical interest; however, it represents the first step toward the implementation of an effective ROM for the parametric problem. Note that during the offline stage we store the state variables in a subset of the time steps and we do not store internal variables: this choice is motivated by the fact that for practical problems memory constraints might prevent the storage of all snapshots; in addition, internal variables might not be computed explicitly by available HF codes.

3.1.1 | Data compression

We resort to POD based on the method of snapshots (cf. Reference 28) to generate the ROB $\underline{Z}$. Given the snapshots $\{\underline{U}^{(j)}_{\mathrm{hf},\mu}\}_{j\in \mathtt{I}_\mathrm{s}} = \{\underline{U}^{(k)}\}_{k=1}^{K}$, $K = |\mathtt{I}_\mathrm{s}|$, we define the Gramian matrix $\mathbf{C} \in \mathbb{R}^{K,K}$ such that $\mathbf{C}_{k,k'} = (\underline{U}^k, \underline{U}^{k'})$; then, we define the POD eigenpairs

$$\mathbf{C}\widetilde{\boldsymbol{\xi}}_n = \lambda_n \widetilde{\boldsymbol{\xi}}_n, \quad \lambda_1 \geq \lambda_2 \geq \cdots \geq \lambda_K \geq 0;$$

finally, we define the POD modes

$$\underline{\zeta}_n := \sum_{k=1}^{K} \left(\widetilde{\boldsymbol{\xi}}_n\right)_k \underline{U}_k, \quad n = 1, \ldots, N.$$

The reduced space size N can be chosen according to the energy criterion:

$$N := \min\left\{ M : \sum_{n=1}^{M} \lambda_n \geq (1 - \mathrm{tol}^2_{\mathrm{POD}}) \sum_{i=1}^{K} \lambda_i \right\}, \tag{8}$$

for some user-defined tolerance $\mathrm{tol}_{\mathrm{POD}} > 0$. Note that the POD modes depend on the choice of the inner product $(\cdot,\cdot)$: we discuss the choice of $(\cdot,\cdot)$ for the THM problem considered in this article in Section 4.

3.1.2 | Hyper-reduction

We denote by $\widehat{\mathbf{R}}^{\mathrm{hf}}_\mu(\cdot)$ and $\widehat{\mathbf{R}}^{\mathrm{eq}}_\mu(\cdot)$ the algebraic reduced residuals associated with the HF and empirical quadrature rules, such that

$$\begin{cases} \left(\widehat{\mathbf{R}}^{\mathrm{hf}}_\mu\left(\boldsymbol{\alpha};\ \boldsymbol{\beta}, \underline{\mathbf{W}}'\right)\right)_n := \mathcal{R}^{\mathrm{hf}}_\mu\left(\underline{\mathbf{Z}}\ \boldsymbol{\alpha},\ \underline{\mathbf{Z}}\ \boldsymbol{\beta},\ \underline{\mathbf{W}}^\star_\mu,\ \underline{\mathbf{W}}',\ \underline{\zeta}_n\right), \quad n = 1, \ldots, N, \\ \left(\widehat{\mathbf{R}}^{\mathrm{eq}}_\mu\left(\boldsymbol{\alpha}; \boldsymbol{\beta}, \underline{\mathbf{W}}'\right)\right)_n := \mathcal{R}^{\mathrm{eq}}_\mu\left(\underline{\mathbf{Z}}\ \boldsymbol{\alpha},\ \underline{\mathbf{Z}}\ \boldsymbol{\beta},\ \underline{\mathbf{W}}^\star_\mu,\ \underline{\mathbf{W}}',\ \underline{\zeta}_n\right), \quad n = 1, \ldots, N, \end{cases}$$

where $\boldsymbol{\alpha}, \boldsymbol{\beta} \in \mathbb{R}^N$, $\underline{\mathbf{W}}' \in \mathbb{R}^{n_\mathrm{q}, N_\mathrm{e}, D_{\mathrm{int}}}$, and $\underline{\mathbf{W}}^\star_\mu = \underline{\mathbf{W}}^\star_\mu\left(\boldsymbol{\alpha}, \boldsymbol{\beta}; \underline{\mathbf{W}}'\right)$ is obtained by substituting in $(4)_3$. We further introduce the Jacobians $\mathbf{J}^{\mathrm{hf}}_\mu(\cdot), \mathbf{J}^{\mathrm{eq}}_\mu(\cdot)$ such that

$$\left(\mathbf{J}^{\mathrm{hf}}_\mu(\boldsymbol{\alpha}; \boldsymbol{\beta}, \underline{\mathbf{W}}')\right)_{n,n'} := \frac{\partial}{\partial \alpha_{n'}} \left(\widehat{\mathbf{R}}^{\mathrm{hf}}_\mu\left(\boldsymbol{\alpha}; \boldsymbol{\beta}, \underline{\mathbf{W}}'\right)\right)_n, \quad \left(\mathbf{J}^{\mathrm{eq}}_\mu(\boldsymbol{\alpha}; \boldsymbol{\beta}, \underline{\mathbf{W}}')\right)_{n,n'} := \frac{\partial}{\partial \alpha_{n'}} \left(\widehat{\mathbf{R}}^{\mathrm{eq}}_\mu\left(\boldsymbol{\alpha}; \boldsymbol{\beta}, \underline{\mathbf{W}}'\right)\right)_n,$$

for $n, n' = 1, \ldots, N$. We observe that the computation of the Jacobian involves the derivatives with respect to the constitutive laws in $\underline{\mathcal{F}}^{\mathrm{hf}}$; we further observe that the residuals $\widehat{\mathbf{R}}^{\mathrm{hf}}_\mu(\cdot)$ and $\widehat{\mathbf{R}}^{\mathrm{eq}}_\mu(\cdot)$ satisfy

$$\widehat{\mathbf{R}}^{\mathrm{hf}}_\mu\left(\boldsymbol{\alpha}; \boldsymbol{\beta}, \underline{\mathbf{W}}'\right) = \mathbf{G}\left(\boldsymbol{\alpha}; \boldsymbol{\beta}, \underline{\mathbf{W}}'\right)\ \boldsymbol{\rho}^{\mathrm{hf}}, \quad \widehat{\mathbf{R}}^{\mathrm{eq}}_\mu\left(\boldsymbol{\alpha}; \boldsymbol{\beta}, \underline{\mathbf{W}}'\right) = \mathbf{G}\left(\boldsymbol{\alpha}; \boldsymbol{\beta}, \underline{\mathbf{W}}'\right)\ \boldsymbol{\rho}^{\mathrm{eq}}, \tag{9}$$

where $\mathbf{G} \in \mathbb{R}^{N, N_\mathrm{e}}$ can be explicitly derived using the same approach as in Reference 8 and $\boldsymbol{\rho}^{\mathrm{hf}} = [1, \ldots, 1]^T$.

As in Reference 6, we reformulate the problem of finding the sparse weights $\boldsymbol{\rho}^{\mathrm{eq}} \in \mathbb{R}^{N_{\mathrm{e}}}$ as the problem of finding a vector $\boldsymbol{\rho}^{\mathrm{eq}}$ such that:

1. the number of nonzero entries in $\boldsymbol{\rho}^{\mathrm{eq}}$, which we denote by $\|\boldsymbol{\rho}^{\mathrm{eq}}\|_0$, is as small as possible;
2. the entries of $\boldsymbol{\rho}^{\mathrm{eq}}$ are non-negative;
3. (*constant-function constraint*) the constant function is integrated accurately: $\left|\sum_{k=1}^{N_{\mathrm{e}}} \rho_k^{\mathrm{eq}} |\mathrm{D}_k| - |\Omega|\right| \ll 1$;
4. (*manifold accuracy constraint*) the empirical and hf residuals are close at operating conditions:

$$\left\| \left(\mathbf{J}_\mu^{\mathrm{hf}}(\boldsymbol{\alpha}_{\mathrm{train}}^{(j)}, \boldsymbol{\alpha}_{\mathrm{train}}^{(j)}; \underline{\mathbf{W}}_{\mathrm{train}}^{(j-1)}) \right)^{-1} \left(\widehat{\mathbf{R}}_\mu^{\mathrm{hf}} \left(\boldsymbol{\alpha}_{\mathrm{train}}^{(j)}, \boldsymbol{\alpha}_{\mathrm{train}}^{(j)}; \underline{\mathbf{W}}_{\mathrm{train}}^{(j-1)} \right) - \widehat{\mathbf{R}}_\mu^{\mathrm{eq}} \left(\boldsymbol{\alpha}_{\mathrm{train}}^{(j)}, \boldsymbol{\alpha}_{\mathrm{train}}^{(j)}; \underline{\mathbf{W}}_{\mathrm{train}}^{(j-1)} \right) \right) \right\|_2 \ll 1, \tag{10}$$

for $j \in \mathtt{I}_{\mathrm{s}}$ and for suitable choices of $\{\boldsymbol{\alpha}_{\mathrm{train}}^{(j)}\}_j$ and $\{\underline{\mathbf{W}}_{\mathrm{train}}^{(j)}\}_j$ that are discussed at the end of the section.

We observe that a similar problem was already introduced in References 4 and 9. Compared to these works, we here add the constant-function constraint that is found to improve the accuracy of the weights when the integrals are close to zero due to the cancelation of the function to be integrated in different parts of the domain (cf. Reference 6).

Exploiting (9), we can restate the previous requirements as a sparse representation problem:

$$\text{find } \boldsymbol{\rho}^{\mathrm{eq}} \in \arg\min_{\boldsymbol{\rho} \in \mathbb{R}^{N_{\mathrm{e}}}} \|\boldsymbol{\rho}\|_0 \text{ s.t. } \begin{cases} \boldsymbol{\rho} \geq \mathbf{0}, \\ \|\mathbf{C}\boldsymbol{\rho} - \mathbf{b}\|_* \leq \delta, \end{cases} \tag{11}$$

for a suitable choices of the matrix $\mathbf{C}$, the vector $\mathbf{b}$, the norm $\|\cdot\|_*$, and the tolerance δ. Since the optimization problem (11) is NP-hard, several authors have proposed computational methods to find approximate solutions to (11) in polynomial time. To provide concrete references, Reference 6 considers a ℓ^1 relaxation of (11) with $\|\cdot\|_\star = \|\cdot\|_{\ell^\infty}$, and resorts to linear programming to find an approximate solution; here, following Farhat et al.,[4] we approximate the solution to (11) by solving the inexact non-negative least squares (NNLS) problem

$$\min_{\boldsymbol{\rho} \in \mathbb{R}^{N_{\mathrm{e}}}} \|\mathbf{C}\boldsymbol{\rho} - \mathbf{b}\|_2 \text{ s.t. } \boldsymbol{\rho} \geq \mathbf{0}. \tag{12}$$

A thorough comparison between the reduced quadrature approaches in References 4 and 6 is beyond the scope of this article; we refer to Reference 29 for a detailed analysis of the performance of NNLS and a comparison with LP for a stochastic sparse representation problem with Gaussian disturbances.

In this work, we rely on the Matlab function `lsqnonneg` that implements the Greedy algorithm proposed in Reference 30 and takes as input the matrix $\mathbf{C}$, the vector $\mathbf{b}$, and a tolerance $\mathrm{tol}_{\mathrm{eq}}$:

$$\boldsymbol{\rho}^{\mathrm{eq}} = \mathtt{lsqnonneg}(\mathbf{C}, \mathbf{b}, \mathrm{tol}_{\mathrm{eq}}).$$

The same algorithm to find the sparse weights $\boldsymbol{\rho}^{\mathrm{eq}}$ given the matrices $\mathbf{C}, \mathbf{b}$ has been first considered in Reference 4: for large-scale problems, a parallelized extension of the algorithm was introduced and successfully applied to hyper-reduction in Reference 31.

Remark 2. The presence of internal variables complexifies the application of EQ procedures. Indeed, the problem formulation in Equation (4) (and Equation (31) for the specific problem of interest) shows the dependence of the residual on state and internal variables both at the current time and at the previous time step. Therefore, in order to compute the entries of $\mathbf{C}, \mathbf{b}$ associated with (10), we should prescribe the triplets $\left\{ \left(\boldsymbol{\alpha}_{\mathrm{train}}^{(j)}, \boldsymbol{\alpha}_{\mathrm{train}}^{(j-1)}, \underline{\mathbf{W}}_{\mathrm{train}}^{(j-1)} \right) \right\}_{j \in \mathtt{I}_{\mathrm{s}}}$: knowledge of the primary and internal variables at time j and $j-1$ for $j \in \mathtt{I}_s$ is thus necessary to construct residuals at each time step.

A first option, which was considered in Reference 9, is to store state and internal variables $\{\underline{U}_{\mathrm{hf}}^{(j)}, \underline{U}_{\mathrm{hf}}^{(j-1)}, \underline{W}_{\mathrm{hf}}^{(j-1)}\}$ at all select time steps $j \in \mathtt{I}_s$. This choice might lead to very large offline memory costs—which scale with $\left(n_{\mathrm{q}} N_{\mathrm{e}} D_{\mathrm{int}} + 2\mathcal{N} D_{\mathrm{eq}}\right) |\mathtt{I}_{\mathrm{s}}|$—and it might require modifications to the HF solver, but it does not require the solution to the ROM with HF quadrature.

An alternative approach, which is considered in this work, is to use HF data to build the ROB for the state variables, solve the ROM (7) with HF quadrature to obtain $\{\widehat{\boldsymbol{\alpha}}_{\mathrm{hf},\mu}^{(j)}, \widehat{\underline{\mathbf{W}}}_{\mathrm{hf},\mu}^{(j)}\}_j$, and then set $\boldsymbol{\alpha}_{\mathrm{train}}^{(j)} = \widehat{\boldsymbol{\alpha}}_{\mathrm{hf},\mu}^{(j)}$ and $\underline{\mathbf{W}}_{\mathrm{train}}^{(j)} = \widehat{\underline{\mathbf{W}}}_{\mathrm{hf},\mu}^{(j)}$. This choice

contributes to reduce offline memory costs and might also avoid modifications to the HF solver; however, it increases offline computational costs. In the numerical results (cf. Table 5), we report computational costs of ROM solves based on HF and empirical quadrature.

We emphasize that the other pieces of our approach—Galerkin projection, POD-Greedy algorithm, time-averaged residual indicator—can cope with both strategies. The decision should thus be based on the particular software architecture considered and on the design constraints.

3.2 | Parametric problem

In order to extend our methodology to parametric problems, we should address two challenges. First, we should explore the parameter domain $\mathcal{P}$ in an efficient way; second, we should devise a compression strategy to combine information from different parameters.

In this work we propose an adaptive strategy based on an inexpensive error indicator described in Section 3.2.2. Our point of departure is the POD-Greedy algorithm proposed in Reference 18. Algorithm 2 summarizes the procedure: the procedure takes as input a discretization of $\mathcal{P}$, Ξ_{train}, a tolerance tol_{loop} for the outer greedy loop, a tolerance tol_{pod} for the data compression step, and the maximum number of greedy iterations $N_{\text{count,max}}$—we here prescribe the termination condition based on the error indicator; we refer to the pMOR literature for other termination conditions.

We observe that the algorithm depends on several building blocks. The FE solver

$$\left[\{\underline{\mathbf{U}}^{(j)}_{\text{hf},\mu}\}_{j\in \mathtt{I}_s}\right] = \texttt{FE-solve}(\mu)$$

takes as input the vector of parameters and returns the snapshot set associated with the sampling times $\mathtt{I}_s \subset \{1, \dots, J_{\max}\}$ (without saving internal variables, as pointed out in Remark 2). The data compression routine

$$\left[\underline{Z}',\ \lambda'\right] = \texttt{data-compression}\left(\underline{Z},\ \lambda, \{\underline{\mathbf{U}}^{(j)}_{\text{hf},\mu^\star}\}_{j\in \mathtt{I}_s}, (\cdot,\cdot), \text{tol}_{\text{pod}}\right)$$

takes as input the current ROB and the POD eigenvalues $\lambda = [\lambda_1, \dots, \lambda_N]^T$, and returns the updated ROB $\underline{Z}'$ and the updated eigenvalues λ'; finally, we observe that construction of the ROM comprises both the construction of the Galerkin ROM and of the error indicator. In the remainder of this section, we discuss each element of the procedure.

Algorithm 2. POD-Greedy algorithm

Require: $\Xi_{\text{train}} = \{\mu^{(k)}\}_{k=1}^{n_{\text{train}}}$, tol_{loop}, tol_{pod}, $N_{\text{count,max}}$.

1: $\mathcal{Z} = \emptyset$, $\lambda = \emptyset$, $\mu^\star = \mu^{(1)}$.
2: **for** $n_{\text{count}} = 1, \dots, N_{\text{count,max}}$ **do**
3: $\left[\{\underline{\mathbf{U}}^{(j)}_{\text{hf},^\star}\}_{j\in \mathtt{I}_s}\right] = \texttt{FE-solve}(\mu^\star)$;
4: $\left[\underline{Z},\ \lambda\right] = \texttt{data-compression}(\underline{Z},\ \lambda, \{\underline{\mathbf{U}}^{(j)}_{\text{hf},^\star}\}_{j\in \mathtt{I}_s}, (\cdot,\cdot), \text{tol}_{\text{pod}})$; ▷ Section 3.2.1.
5: Construct the ROM with error indicator. ▷ Section 3.2.3.
6: **for** $j = 1 : n_{\text{train}}$ **do**
7: Solve the ROM (7) for $\mu = \mu^{(k)}$ and compute Δ_μ.
8: **end for**
9: $\mu^\star = \arg\max_{\mu\in\Xi_{\text{train}}} \Delta_\mu$ ▷ Greedy search
10: **if** $\Delta_{\mu^\star} < \text{tol}_{\text{loop}}$ **then**, ▷ Termination condition
11: `break`,
12: **end if**.
13: **end for**
14: **return** ROB $\underline{Z}$ and ROM: $\mu \in \mathcal{P} \mapsto \{\widehat{\boldsymbol{\alpha}}^{(j)}_\mu\}_{j=1}^{J_{\max}}$.

3.2.1 | Data compression

We consider two different data compression strategies: a hierarchical POD (H-POD) and a hierarchical approximate POD (HAPOD). Both techniques have been considered in several previous works: we refer to Reference 32, Section 3.5 for H-POD and to Reference 33 for HAPOD; HAPOD is also related to incremental singular value decomposition in linear algebra.[34] Here, we review the two approaches for completeness. We denote by $\Pi_{\mathcal{Z}} : \mathcal{X}_{\text{hf}} \to \mathcal{Z}$ the orthogonal projection operator on $\mathcal{Z} \subset \mathcal{X}_{\text{hf}}$; furthermore, we introduce notation

$$\left[\underline{Z},\ \lambda\right] = \texttt{POD}\left(\{\underline{U}^{(k)}\}_{k=1}^{K}, (\cdot,\cdot), \text{tol}_{\text{pod}}\right)$$

to refer to the application of POD to the snapshot set $\{\underline{U}^{(k)}\}_{k=1}^{K}$, with inner product $(\cdot,\cdot)$, and tolerance tol_{pod} (cf. (8)), with $\underline{Z} = [\underline{\zeta}_1, \dots, \underline{\zeta}_N]$, $\|\underline{\zeta}_n\| = 1$, $\lambda = [\lambda_1, \dots, \lambda_N]^T$, and $\lambda_1 \geq \lambda_2 \geq \cdots \geq \lambda_N$.

Given $\underline{Z}$ and the snapshots $\{\underline{U}^{(j)}_{\text{hf},\mu^\star}\}_j$ H-POD considers the update:

$$\underline{Z}' = \left[\underline{Z}, \underline{Z}^{\text{new}}\right], \quad \underline{Z}^{\text{new}} = \texttt{POD}\left(\{\Pi_{\mathcal{Z}^\perp}\underline{U}^{(j)}_{\text{hf},\mu^\star}\}_j, (\cdot,\cdot), \text{tol}_{\text{pod}}\right). \tag{13a}$$

Note that the approach does not require to input the POD eigenvalues λ from the previous iterations. We observe that the approach leads to a sequence of nested spaces—that is, the updated ROB contains the ROB of the previous iteration—and it returns an orthonormal basis of the reduced space. In our experience, the choice of the tolerance tol_{pod} is extremely challenging: since (8) depends on the relative energy content of the snapshot set, the update (13a) with fixed tolerance tol_{pod} might lead to an excessively large (resp., small) number of modes when $\max_j \|\underline{U}^{(j)}_{\text{hf},\mu^\star} - \Pi_{\mathcal{Z}}\underline{U}^{(j)}_{\text{hf},\mu^\star}\|$ is small (resp., large). For this reason, we propose to choose the number of new modes N^{new} using the criterion:

$$N^{\text{new}} := \min\left\{M \ :\ \max_{j\in \mathtt{I}_s} \frac{\|\Pi_{(\mathcal{Z}\oplus\mathcal{Z}_M^{\text{new}})^\perp}\underline{U}^{(j)}_{\text{hf},\mu^\star}\|}{\|\underline{U}^{(j)}_{\text{hf},\mu^\star}\|} \leq \text{tol}_{\text{pod}},\ \ \mathcal{Z}_M^{\text{new}} = \text{span}\{\underline{\zeta}_m^{\text{new}}\}_{m=1}^{M}\right\}. \tag{13b}$$

Note that this choice enforces that the in-sample relative projection error is below a certain threshold for all snapshots computed during the greedy iterations.

HAPOD considers the update

$$[\underline{Z}', \lambda'] = \texttt{POD}\left(\{\underline{U}^{(j)}_{\text{hf},\mu^\star}\}_j \cup \{\lambda_n\underline{\zeta}_n\}_{n=1}^{N}, (\cdot,\cdot), \text{tol}_{\text{pod}}\right). \tag{14}$$

Note that the approach (14) does not in general lead to hierarchical (nested) spaces. As discussed in Reference 33, Section 3.3, which refers to (14) as to *distributed HAPOD*, it is possible to relate the performance of the reduced space obtained using HAPOD to the performance of the POD space associated with the snapshot set $\{\underline{U}^{(j)}_{\text{hf},\mu^{\star,n}} : n = 1, \dots, N_{\text{count,max}},\ j \in \mathtt{I}_s\}$: we refer to the above-mentioned paper for a thorough discussion.

3.2.2 | Time-averaged error indicator

We define the trajectories $\mathbb{U} = \{\underline{U}^{(j)}\}_{j=1}^{J_{\max}}$ and $\mathbb{W} = \{\underline{W}^{(j)}\}_{j=1}^{J_{\max}}$; given the pair $(\mathbb{U}, \mathbb{W})$, we define the time-average residual:

$$\mathcal{R}^{\text{hf}}_{\text{avg},\mu}\left(\mathbb{U}, \mathbb{W}, \underline{V}\right) := \sum_{j=1}^{J_{\max}} (t^{(j)} - t^{(j-1)})\, \mathcal{R}^{\text{hf}}_{\mu}\left(\underline{U}^{(j)}, \underline{U}^{(j-1)}, \underline{W}^{(j)}, \underline{W}^{(j-1)}, \underline{V}\right), \quad \forall\, \underline{V} \in \mathcal{X}_{\text{hf},0}, \tag{15}$$

and the error indicator

$$\Delta^{\text{hf}}_{\mu}(\mathbb{U}, \mathbb{W}) = \sup_{\underline{V}\in\mathcal{X}_{\text{hf},0}} \frac{\mathcal{R}^{\text{hf}}_{\text{avg},\mu}\left(\mathbb{U}, \mathbb{W}, \underline{V}\right)}{\|\underline{V}\|}. \tag{16}$$

The indicator (16) is expensive to evaluate since it relies on hf quadrature and it requires the computation of the supremum over all elements of $\mathcal{X}_{\mathrm{hf},0}$: following Reference 35, we consider the hyper-reduced error indicator

$$\Delta_\mu(\mathbb{U},\mathbb{W}) = \sup_{\underline{V}\in\mathcal{Y}} \frac{\mathcal{R}^{\mathrm{eq,r}}_{\mathrm{avg},\mu}\left(\mathbb{U},\mathbb{W},\underline{V}\right)}{\|\underline{V}\|}, \tag{17}$$

where $\mathcal{Y}\subset\mathcal{X}_{\mathrm{hf},0}$ is an M-dimensional empirical test space, while $\mathcal{R}^{\mathrm{eq,r}}_{\mathrm{avg},\mu}$ is defined by replacing $\mathcal{R}^{\mathrm{hf}}_{\mu}$ in (15) with a suitable sparse weighted residual of the form (7a), defined over the elements $\mathtt{I}_{\mathrm{eq,r}}\subset\{1,\dots,N_{\mathrm{e}}\}$.

Given the ROM solution $(\widehat{\mathbb{U}}_\mu,\widehat{\mathbb{W}}_\mu)$, the test space $\mathcal{Y}$ should guarantee that

$$\sup_{\underline{V}\in\mathcal{Y}} \frac{\mathcal{R}^{\mathrm{hf}}_{\mathrm{avg},\mu}\left(\widehat{\mathbb{U}}_\mu,\widehat{\mathbb{W}}_\mu,\underline{V}\right)}{\|\underline{V}\|} \approx \sup_{\underline{V}\in\mathcal{X}_{\mathrm{hf},0}} \frac{\mathcal{R}^{\mathrm{hf}}_{\mathrm{avg},\mu}\left(\widehat{\mathbb{U}}_\mu,\widehat{\mathbb{W}}_\mu,\underline{V}\right)}{\|\underline{V}\|}, \quad \forall\mu\in\mathcal{P}, \tag{18}$$

which implies that $\mathcal{Y}$ should be an approximation of the space of Riesz elements $\mathcal{M}_{\mathrm{test}} := \{\underline{\widehat{\psi}}_\mu \ : \ \mu\in\mathcal{P}\}$ with

$$\left(\underline{\widehat{\psi}}_\mu,\underline{V}\right) = \mathcal{R}^{\mathrm{hf}}_{\mathrm{avg},\mu}\left(\widehat{\mathbb{U}}_\mu,\widehat{\mathbb{W}}_\mu,\underline{V}\right), \quad \forall\,\underline{V}\in\mathcal{X}_{\mathrm{hf},0}. \tag{19}$$

On the other hand, the empirical quadrature rule should ensure that

$$\mathcal{R}^{\mathrm{eq,r}}_{\mathrm{avg},\mu}\left(\widehat{\mathbb{U}}_\mu,\widehat{\mathbb{W}}_\mu,\underline{\psi}_m\right) \ \approx \ \mathcal{R}^{\mathrm{hf}}_{\mathrm{avg},\mu}\left(\widehat{\mathbb{U}}_\mu,\widehat{\mathbb{W}}_\mu,\underline{\psi}_m\right), \quad \forall\ \mu\in\mathcal{P},\ m=1,\dots,M, \tag{20}$$

where $\underline{\psi}_1,\dots,\underline{\psi}_M$ is an orthonormal basis of $\mathcal{Y}$.

In our implementation, we compute the error indicator during the time iterations—as opposed to after having computed the whole solution trajectory. Algorithm 3 provides the complete online solution and residual indicator computations. We find that computation of Δ_μ requires to compute the internal variables $\widehat{\mathbb{W}}_\mu$ in the elements $\mathtt{I}_{\mathrm{eq}}\cup\mathtt{I}_{\mathrm{eq,r}}$ at each time iteration (cf. 7b), and it requires to store the trial ROB $\underline{Z}$ in $\{\mathtt{D}_k : k\in\mathtt{I}_{\mathrm{eq}}\cup\mathtt{I}_{\mathrm{eq,r}}\}$ and the test basis $\underline{Y}=[\underline{\psi}_1,\dots,\underline{\psi}_M]$ in $\{\mathtt{D}_k : k\in\mathtt{I}_{\mathrm{eq,r}}\}$.

Algorithm 3. Online solution and residual computations

1: Initial state and internal variables; set $\widehat{\mathbf{R}}^{\mathrm{avg}}_\mu = \mathbf{0}$.
2: **for** $j=1,\dots,J_{\max}$ **do**
3: Compute $\widehat{\boldsymbol{\alpha}}^{(j)}_\mu$ by solving (7b).
4: Compute $\left(\underline{\widehat{\mathbf{W}}}^{(j)}_\mu\right)_{\cdot,k,\cdot}$ for all $k\in\mathtt{I}_{\mathrm{eq,r}}$ using $(7\mathrm{b})_2$.
5: Assemble $\widehat{\mathbf{R}}^{(j)}_\mu\in\mathbb{R}^M$ such that $\left(\widehat{\mathbf{R}}^{(j)}_\mu\right)_m = \mathcal{R}^{\mathrm{eq,r}}_\mu\left(\underline{\widehat{U}}^{(j)}_\mu,\ \underline{\widehat{U}}^{(j-1)}_\mu,\ \underline{\widehat{W}}^{(j)}_\mu,\ \underline{\widehat{W}}^{(j-1)}_\mu,\ \underline{\psi}_m\right)$ for $m=1,\dots,M$.
6: Update $\widehat{\mathbf{R}}^{\mathrm{avg}}_\mu = \widehat{\mathbf{R}}^{\mathrm{avg}}_\mu + (t^{(j)}-t^{(j-1)})\widehat{\mathbf{R}}^{(j)}_\mu$.
7: **end for**
8: **return** $\{\widehat{\boldsymbol{\alpha}}^{(j)}_\mu\}_j$ and $\Delta_\mu = \|\widehat{\mathbf{R}}^{\mathrm{avg}}_\mu\|_2$

Several authors (e.g., Reference 18) have considered the time-discrete $L^2(0,T_{\mathrm{f}};\mathcal{X}'_{\mathrm{hf},0})$ residual indicator

$$\Delta^{\mathrm{hf},2}_\mu(\mathbb{U},\mathbb{W}) = \sqrt{\sum_{j=1}^{J_{\max}}(t^{(j)}-t^{(j-1)})\left(\sup_{\underline{V}\in\mathcal{X}_{\mathrm{hf},0}} \frac{\mathcal{R}^{\mathrm{hf}}_\mu\left(\underline{U}^{(j)},\underline{U}^{(j-1)},\underline{W}^{(j)},\underline{W}^{(j-1)},\underline{V}\right)}{\|\underline{V}\|}\right)^2}. \tag{21}$$

We observe that we could apply the same ideas considered in this section to devise an hyper-reduced counterpart of the residual indicator (21). However, we find that the test space $\mathcal{Y}$ and the empirical quadrature rule should be accurate for all parameters and for all time steps: as a result, the resulting test space $\mathcal{Y}$ might be significantly higher dimensional and the quadrature rule might be significantly less sparse, for the desired accuracy. For this reason, in this work, we investigate the effectivity of the time-averaged error indicator (17).

3.2.3 | ROM construction

In order to devise an actionable ROM, we should discuss (i) the choice of the EQ rule $\boldsymbol{\rho}^{\text{eq}}$, (ii) the choice of the test space $\mathcal{Y}$ and of the EQ rule $\boldsymbol{\rho}^{\text{eq,r}}$ in (17). In view of the presentation of the computational procedure, we define the ROM solution with hf quadrature $(\widehat{\mathbb{U}}_\mu^{\text{hf}}, \widehat{\mathbb{W}}_\mu^{\text{hf}})$; we denote by $\mathbf{C}_\mu \in \mathbb{R}^{K\cdot N, N_{\text{e}}}$ the EQ matrix associated with the manifold accuracy constraints in (10) for $\mu \in \mathcal{P}$ (cf. Section 3.1.2); we further define the vector $\mathbf{c} = [|\mathtt{D}_1|, \dots, |\mathtt{D}_{N_{\text{e}}}|]^T$ associated with the constant function accuracy constraint. Given the test reduced basis $\underline{\psi}_1, \dots, \underline{\psi}_M$, we define $\mathbf{G}_\mu^{\text{r}} \in \mathbb{R}^{M, N_{\text{e}}}$ such that

$$\left(\mathbf{G}_\mu^{\text{r}} \boldsymbol{\rho}_{\text{hf}}\right)_m = \mathcal{R}_{\text{avg},\mu}^{\text{eq,r}}\left(\widehat{\mathbb{U}}_\mu^{\text{hf}}, \widehat{\mathbb{W}}_\mu^{\text{hf}}, \underline{\psi}_m\right), \quad \forall\, \mu \in \mathcal{P},\ m = 1, \dots, M. \tag{22}$$

We further define the unassembled average residual $\mathbf{R}_\mu^{\text{avg,un}} \in \mathbb{R}^{n_{\text{ip}}, N_{\text{e}}, D_{\text{eq}}}$: we observe that $\mathbf{R}_\mu^{\text{avg,un}}$ might be employed to build the FE residual and ultimately compute the Riesz representers $\underline{\widehat{\psi}}_\mu$ in (19), and also, given $\mathcal{Y}$, to compute $\mathbf{G}_\mu^{\text{r}}$.

We focus on the construction of the ROM at the n_{c}th iteration of the POD Greedy algorithm. We define $\Xi^\star = \{\tilde{\mu}^{(j)}\}_{j=1}^{n_{\text{rom}}} = \{\mu^{\star,(i)}\}_{i=1}^{n_{\text{c}}} \cup \{\tilde{\mu}^{(j)}\}_{j=1}^{n_{\text{train,eq}}}$, where $\mu^{\star,(1)}, \dots, \mu^{\star,(n_{\text{c}})}$ are the parameters sampled by the greedy algorithm and $\tilde{\mu}^{(1)}, \dots, \tilde{\mu}^{(n_{\text{train,eq}})}$ are independent identically distributed samples from the uniform distribution over $\mathcal{P}$. Algorithm 4 summarizes the computational procedure as implemented in our code. The test space $\mathcal{Y}$ is built using POD as in Reference 35, while the EQ weights $\underline{\rho}_{\text{eq},r}$ are obtained using the non-negative least-squares method.

Algorithm 4. Construction of the ROM

1: **for** $\mu \in \Xi^\star$ **do**
2: Solve the ROM with hf quadrature and compute $\mathbf{C}_\mu$ and $\mathbf{R}_\mu^{\text{avg,un}}$.
3: **end for**
4: Assemble $\mathbf{C} = \begin{bmatrix} \mathbf{C}_{\tilde{\mu}^{(1)}} \\ \vdots \\ \mathbf{C}_{\tilde{\mu}^{(n_{\text{rom}})}} \\ \mathbf{c}^T \end{bmatrix} \in \mathbb{R}^{K\cdot N\cdot n_{\text{rom}}, N_{\text{e}}}$ and set $\boldsymbol{\rho}^{\text{eq}} = \mathtt{lsqnonneg}(\mathbf{C}, \mathbf{C}\boldsymbol{\rho}^{\text{hf}}, \text{tol}_{\text{eq}})$.
5: Compute the Riesz representers $\{\underline{\widehat{\psi}}_\mu\}_{\mu\in\Xi_\star}$ using (19).
6: Define the empirical test space $\mathcal{Y} = \text{span}\{\underline{\psi}_m\}_{m=1}^M$ as $[\{\underline{\psi}_m\}_{m=1}^M] = \mathtt{POD}\left(\{\underline{\widehat{\psi}}_\mu\}_{\mu\in\Xi_\star}, (\cdot,\cdot), \text{tol}_{\text{pod,res}}\right)$.
7: Assemble $\mathbf{G} = \begin{bmatrix} \mathbf{G}_{\tilde{\mu}^{(1)}} \\ \vdots \\ \mathbf{G}_{\tilde{\mu}^{(n_{\text{rom}})}} \\ \mathbf{c}^T \end{bmatrix} \in \mathbb{R}^{M\cdot n_{\text{rom}}, N_{\text{e}}}$ and set $\boldsymbol{\rho}^{\text{eq,r}} = \mathtt{lsqnonneg}(\mathbf{G}, \mathbf{G}\boldsymbol{\rho}^{\text{hf}}, \text{tol}_{\text{eq,r}})$.

4 | THM MODEL PROBLEM

In this section, we illustrate the non-dimensional mathematical formulation and the numerical discretization of the THM system considered in this work. We assume that the solid undergoes small displacements and that soil is fully saturated in water. We resort to a Lagrangian formulation for the solid, and to an Eulerian formulation for the fluid.

4.1 | Preliminary definitions

We first introduce the state variables and the internal variables. The state variables are denoted as $\underline{U}_\mu$ in the continuous formulation in Equation (1), and their FE approximation as $\underline{\mathbf{U}}_\mu^{\mathrm{hf}}$ in the high-fidelity discretization in Equation (4). For the specific problem of interest, $\underline{U} = [\underline{u}^{\mathrm{T}}, p_{\mathrm{w}}, T]^{\mathrm{T}}$: the state variables represent solid displacement, water pressure, and temperature and are reported in Table 1; the internal variables $\underline{W} = [\rho_{\mathrm{w}}, \varphi, h_{\mathrm{w}}, Q, \underline{M}_{\mathrm{w}}^{\mathrm{T}}, m_{\mathrm{w}}]^{\mathrm{T}}$ represent dependent physical quantities and are illustrated in Table 2, together with the corresponding SI units.

We denote the Cauchy stress tensor by $\underline{\underline{\sigma}}$ [Pa], and we define the volumetric deformation $\epsilon_{\mathrm{V}} = tr(\underline{\underline{\epsilon}})$ where $\underline{\underline{\epsilon}}$ is the strain tensor: $\underline{\underline{\epsilon}} = \nabla_{\mathrm{s}}\underline{u} = \frac{1}{2}\left(\nabla\underline{u} + \nabla\underline{u}^{T}\right)$. We also provide in Table 3 the characteristic parameters that we use for the non-dimensionalization.

4.1.1 | Geometry configuration

The computational domain is shown in Figure 1A. The geological repositories, modeled as boundary conditions, are depicted in red at the bottom of the domain, in the case of two activated alveoli. In the vertical (x_2) direction, the domain is split into three layers: a clay layer denoted as UA ("*unité argilleuse*"), a transition layer UT ("*unité de transition*"), and a silt-carbonate layer USC ("*unité silto-carbonatée*").

In Figure 1B, the FE grid is shown. The number of degrees of freedom for the first state component (solid displacement) is $\mathcal{N}^{\mathrm{u}} = 40{,}430$, while for water pressure and temperature is $\mathcal{N}^{\mathrm{p}} = \mathcal{N}^{\mathrm{t}} = 9045$. The grid is refined in the proximity of the

TABLE 1 Primary variables

	SI unit	Description
$\underline{u}$	m	Solid displacement
p_{w}	Pa	Water pressure
T	K	Temperature

TABLE 2 Dependent variables

	SI unit	Label
ρ_{w}	$\mathrm{kg\,m^{-3}}$	Water density
φ	%	Eulerian porosity
h_{w}	$\mathrm{J\,kg^{-1}}$	Mass enthalpy of water
Q	Pa	Non-convected heat
$\underline{M}_{\mathrm{w}}$	$\mathrm{kg\,m^{-2}\,s^{-1}}$	Mass flux
m_{w}	$\mathrm{kg\,m^{-3}}$	Mass input

TABLE 3 Characteristic constants

	SI unit	Value
$\bar{t}$	s	3.15×10^7
$\overline{H}$	m	77.3
σ_0	Pa	11.3×10^6
ρ_0	$\mathrm{kg\,m^{-3}}$	2450
T_{ref}	K	297.5
$\overline{\Delta T}$	K	30

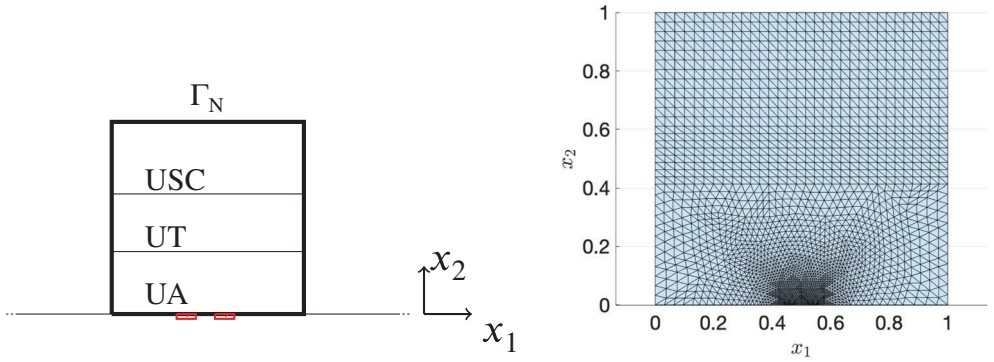

FIGURE 1 Geometric configuration: (A) The non-dimensional domain and (B) the mesh. The size of each alveoulus is equal to $l_Q = 3.09\,\text{m}$, while the distance between consecutive alveoli is equal to $l = 6.18\,\text{m}$

alveoli to better capture the relevant features of the solution. We consider a $\mathtt{p} = 3$ FE discretization for the displacement component, and a $\mathtt{p} = 2$ FE discretization for both pressure and temperature.

4.2 | Mathematical problem

We first state the equilibrium equations—the superscripts $(\cdot)^{\mathrm{m}}, (\cdot)^{\mathrm{n}}, (\cdot)^{\mathrm{t}}$ refer to quantities associated with the mechanical, hydraulic, and thermal behaviors, respectively. Then, we present the constitutive laws that are considered and finally we present the boundary conditions. To clarify the presentation, we report in Table 4 the parameters that enter in the constitutive laws.

We denote by $\underline{F}_{\mathrm{m}} = -\frac{g}{\gamma}\underline{e}_2$ (where $\gamma = \frac{\sigma_0}{\rho_0 H}$) the mechanical force with g defined in Table 4 and we specify that $\underline{n}$ (resp. $\underline{t}$) is the unitary outward normal (resp. tangential) vector in the domain depicted in Figure 1A; then we introduce the equilibrium of mechanical forces:

$$\begin{cases} -\nabla \cdot \underline{\underline{\sigma}} = \rho \underline{F}_{\mathrm{m}} & \text{in } \Omega, \\ \underline{\underline{\sigma}}\,\underline{n} = \underline{g}_{\mathrm{m,N}} & \text{on } \Gamma_{\mathrm{N}}, \\ \underline{u} \cdot \underline{n} = 0 & \text{on } \partial\Omega \setminus \Gamma_{\mathrm{N}}, \\ (\underline{\underline{\sigma}}\,\underline{n}) \cdot \underline{t} = 0 & \text{on } \partial\Omega \setminus \Gamma_{\mathrm{N}}, \end{cases} \tag{23a}$$

where Γ_{N} is depicted in Figure 1A. The Neumann datum $\underline{g}_{\mathrm{m,N}}$ is given by $\underline{g}_{\mathrm{m,N}} = -\underline{e}_2$. The stress tensor is linked to the primary and internal variables by the linear law

$$\underline{\underline{\sigma}} = 2\mu \nabla_{\mathrm{s}} \underline{u} + \left(\lambda\ \nabla \cdot \underline{u}\ -\ (2\mu + 3\lambda)\alpha_{\mathrm{s}} T - b p_{\mathrm{w}}\right) \mathbb{1}, \tag{23b}$$

where the Lamé constants μ', λ satisfy

$$\mu' = \frac{E}{2(1+\nu)},$$
$$\lambda = \frac{E\nu}{(1+\nu)(1-2\nu)},$$

and E and ν are introduced in Table 4.

TABLE 4 Parameters of the constitutive laws

	SI unit	Description	Reference value	Formula
g	$\mathrm{m\,s^{-2}}$	Gravity acceleration	9.81	
E	Pa	Young's modulus	11.4×10^9 UA 12.3×10^9 UT 20×10^9 USC	
ν	%	Poisson's ratio	0.3	
μ	Pa	Lamé parameter		$\frac{E}{2(1+\nu)}$
λ	Pa	Lamé parameter		$\frac{E\nu}{(1+\nu)(1-2\nu)}$
b	%	Biot coefficient	0.6	
α_s	$\mathrm{K^{-1}}$	Solid thermal expansion coefficient	1.28×10^{-5}	
α_0	$\mathrm{K^{-1}}$	Expansion coefficient	1.28×10^{-5}	
κ_w	$\mathrm{m^2}$	Intrinsic permeability of porous medium	10^{-21}	
μ_w	MPa s	Dynamic viscosity		$\mu_w = \mu_{w,0}\exp(\frac{1808.5}{T})$
$\mu_{w,0}$	MPa s	Dynamic viscosity coefficient	2.1×10^{-12}	
K_s	Pa	Bulk modulus of the solid		
K_w	Pa	Bulk modulus of water	2×10^9	$K_s = \frac{E}{3(1-2\nu)}$
C_w^p	$\mathrm{J\,kg^{-1}\,K^{-1}}$	Heat capacity at constant pressure	4180	
K_0	Pa	Drained bulk modulus		$K_0 = (1-b)K_s$
α_w	$\mathrm{K^{-1}}$	Thermal expansion coefficient of water		$\alpha_w = 9.52\times10^{-5}\log(T-273) - 2.19\times10^{-4}$
$\alpha_{w,m}$		Dilation coefficient		
C_σ^s	$\mathrm{J\,kg^{-1}\,K}$	Specific heat at constant stress	537 UA 603 UT 640 USC	
ρ^0	$\mathrm{kg\,m^{-3}}$	Porous medium initial density	2450 UA 2450 UT 2500 USC	
ρ_w^0	$\mathrm{kg\,m^{-3}}$	Initial water density	10^3	
φ^0	%	Initial Eulerian porosity	0.25 UA 0.21 UT 0.19 USC	
h_w^0	$\mathrm{m^2\,s^{-2}}$	Initial water enthalpy		$h_w^0 = \frac{p_w^0 - p_{atm}}{\rho_w^0}$
ρ_s	$\mathrm{kg\,m^{-3}}$	Density ratio		$\rho_s = \frac{\rho^0 - \rho_w^0\varphi^0}{1-\varphi^0}$
C_ϵ^0	$\mathrm{Pa\,K^{-1}}$	Specific heat at constant deformation		$C_\epsilon^0 = (1-\varphi)\rho_s C_\sigma^s + \varphi\rho_w C_w^p - 9TK_0\alpha_s^2$
Λ		Thermic conductivity tensor		$\Lambda = \mathrm{diag}(\lambda_1, \lambda_2)$
λ_1	$\mathrm{W\,m^{-1}\,K^{-1}}$	Thermic conductivity component	1.5 UA 1.5 UT 1.3 USC	

(Continues)

TABLE 4 (Continued)

	SI unit	Description	Reference value	Formula
λ_2	$W\,m^{-1}\,K^{-1}$	Thermic conductivity component	1 UA	
			1 UT	
			1.3 USC	
Θ	$Pa\,s^{-1}$	Volumetric heat sources		

Note: Layers UA, UT, USC are depicted in Figure 1A.

We state the mass conservation of water as follows

$$\begin{cases} \partial_t\, m_{\mathrm{w}} + \nabla \cdot \underline{M}_{\mathrm{w}} = 0 & \text{in } \Omega, \\ \underline{M}_{\mathrm{w}} \cdot \underline{n} = 0 & \text{on } \partial\Omega, \end{cases} \tag{24a}$$

where the mass flux $\underline{M}_{\mathrm{w}}$ is given by the Darcy law

$$\underline{M}_{\mathrm{w}} = -\gamma \left(\nabla p_{\mathrm{w}} - \rho_{\mathrm{w}} \underline{F}_{\mathrm{m}} \right), \tag{24b}$$

and

$$\gamma = \rho_{\mathrm{w}} \frac{\kappa_{\mathrm{w}}\, \sigma_0\, \bar{t}}{\rho_0 \mu_{\mathrm{w},0}\, \overline{H}^2} \exp\left(-\frac{1808.5}{T_{\mathrm{ref}} + \overline{\Delta T}\, T} \right). \tag{24c}$$

Finally, we consider the energy balance:

$$\begin{cases} h_{\mathrm{w}} \partial_t\, m_{\mathrm{w}} + \partial_t\, Q + \nabla \cdot \left(h_{\mathrm{w}} \underline{M}_{\mathrm{w}} + \underline{q} \right) - \underline{M}_{\mathrm{w}} \cdot \underline{F}_{\mathrm{m}} = \Theta & \text{in } \Omega, \\ \left(h_{\mathrm{w}} \underline{M}_{\mathrm{w}} + \underline{q} \right) \cdot \underline{n} = g_{\mathrm{t,N}} & \text{on } \partial\Omega, \end{cases} \tag{25a}$$

where Q is the non-convective heat, $\underline{q}$ is the thermal flux and is given by the Fick law

$$\underline{q} = -\Lambda \nabla T, \tag{25b}$$

with $\Lambda = \mathrm{diag}(\lambda_1, \lambda_2)$. If we denote by $\Gamma_{\mathrm{al}} \subset \partial\Omega$ the region associated with the alveoli, $g_{t,N}$ is equal to

$$g_{t,N} = \frac{P_{\mathrm{t}} n_c \bar{t}}{l_Q \overline{H}^2 \sigma_0} \exp\left(-t/\tau\right) \mathbb{1}_{\Gamma_{\mathrm{al}}} = C_{\mathrm{al}} \exp\left(-t/\tau\right) \mathbb{1}_{\Gamma_{\mathrm{al}}}, \tag{26}$$

where n_c [%] is the density of the radioactive waste stock in each alveolus (equal to 45 anisters), $P_{\mathrm{t}} = 31.4\,\mathrm{W}$ is the unitary termic power at the initial time, $l_Q = 3.09\,\mathrm{m}$ is the size of each alveolus, $\sigma_0, \overline{H}, \bar{t}$ are introduced in Table 3 and $\tau = \frac{\bar{t}}{\log(0.112)}$ [s] is a characteristic decay time.

$$\begin{cases} \dfrac{d\rho_{\mathrm{w}}}{\rho_{\mathrm{w}}} = \dfrac{dp_{\mathrm{w}}}{K_{\mathrm{w}}} - 3\alpha_{\mathrm{w}} dT, & (27a)\\ \dfrac{d\varphi}{b-\varphi} = d\epsilon_{\mathrm{V}} - 3\alpha_{\mathrm{s}} dT + \dfrac{dp_{\mathrm{w}}}{K_{\mathrm{s}}}, & (27b)\\ dh_{\mathrm{w}} = C_{\mathrm{w}}^{\mathrm{p}}\, dT + (\beta_h^{\mathrm{p}} - 3\alpha_{\mathrm{w}} T)\dfrac{dp_{\mathrm{w}}}{\rho_{\mathrm{w}}}, & (27c)\\ \delta Q = \left(\beta_Q^{\epsilon} + 3\alpha_{\mathrm{s}} K_0\, T\right)\, d\epsilon_{\mathrm{V}} - \left(\beta_Q^{\mathrm{p}} + 3\alpha_{\mathrm{w,m}} T\right)\, dp_{\mathrm{w}} + C_{\epsilon}^{0}\, dT, & (27d)\\ m_{\mathrm{w}} = \rho_{\mathrm{w}}(1+\epsilon_{\mathrm{V}})\,\varphi - \rho_{\mathrm{w}}^{0}\varphi^{0}. & (27e) \end{cases}$$

Here, we have $\beta_h^p = 1 - 3\alpha_{\mathrm{w}} T_{\mathrm{ref}}$, $\beta_Q^{\epsilon} = 3\alpha_{\mathrm{s}} K_0 T_{\mathrm{ref}}$, $\beta_Q^p = 3\alpha_{\mathrm{w,m}} T_{\mathrm{ref}}$.
The parameters in (27a)–(27e) are defined in Table 4.

4.2.1 | Initial conditions

To set the initial conditions, we consider the case of deactivated repositories: therefore, we set thermal flux equal to zero and we set a constant temperature $T_0 = T_{\mathrm{ref}}$ in Ω, where the reference temperature is defined in Table 3. We aim at finding the initial values of the primary variables $\underline{u}$ and p_{w} that correspond to the equilibrium solutions of a preliminary problem: here, the Neumann boundary condition for the energy equation is zero, that is, $g_{\mathrm{t,N}} = 0$, and temperature is constant and equal to the reference value T_{ref} (in Table 3).

We then seek $\underline{u}_0$, $p_{\mathrm{w},0}$ such that the initial solution vector $\underline{U}_0 = [\underline{u}_0^{\mathrm{T}}, p_{\mathrm{w}}, T_0]^{\mathrm{T}}$ satisfies the equilibrium equations (23a), (24a), and (25a) with thermal flux $g_{\mathrm{t,N}}$ equal to 0 on the domain boundary $\partial\Omega$. Toward this end, we first observe that (27a) reduces to

$$\frac{d\rho_{\mathrm{w}}}{\rho_{\mathrm{w}}} = \frac{dp_{\mathrm{w}}}{K_{\mathrm{w}}} \tag{28}$$

that brings to $p_{\mathrm{w}} = \rho_{-\infty} \exp\left(\frac{1}{K_{\mathrm{w}}}(p_{\mathrm{w}} - p_{-\infty})\right)$. If we assume that $\rho_{\mathrm{w}} = \rho_{-\infty} = \rho_{\mathrm{w},0}$, we find $p_{\mathrm{w}} = p_{-\infty}$; furthermore, by substituting these assumptions into the hydraulic equilibrium equation we find

$$p_{\mathrm{w},0}(x,y) = p_{\mathrm{w,top}} + \rho_{\mathrm{w},0} g(1-y), \tag{29}$$

where $p_{\mathrm{w,top}}$ is a datum for water pressure that is defined at the top boundary of the domain $(0,1)\times\{1\}$. Finally, we search for $\underline{u}_0$ as the solution to the equilibrium equation of mechanical forces:

$$\int_\Omega 2\mu\, \nabla_{\mathrm{s}}\, \underline{u}_0 \;:\; \nabla_{\mathrm{s}}\, \underline{v} + \lambda(\nabla\cdot\underline{u}_0)(\nabla\cdot\underline{v}) - b p_{\mathrm{w},0}\, \nabla\cdot\underline{v} - \rho^0 \underline{F}_{\mathrm{m}}\cdot\underline{v}\, dx = \int_{\Gamma_{\mathrm{N}}} \underline{g}_{\mathrm{m,N}}\cdot\underline{v}\, dx, \tag{30}$$

for all $\underline{v} \in \mathcal{X}_{\mathrm{hf}}^{\mathrm{u}}$, such that $\underline{v}\cdot\underline{n}|_{\partial\Omega\setminus\Gamma_{\mathrm{N}}} = 0$.

4.3 | FE formulation

We resort to an implicit Euler time discretization scheme, with $J_{\max} = 100$ uniform time steps; the superscript $(\cdot)^+$ refers to the new solution (at the current time step j, for $j = 1, \ldots, J_{\max}$), while $(\cdot)^-$ refers to the solution at the previous time steps:

$$\begin{cases} \int_\Omega 2\mu\, \nabla_{\mathrm{s}}\, \underline{u}^+ \;:\; \nabla_{\mathrm{s}}\, \underline{v} + \left(\lambda\nabla\cdot\underline{u}^+ - (2\mu+3\lambda)\,\alpha_{\mathrm{s}} T^+ - b p_{\mathrm{w}}^+\right)\, \nabla\cdot\underline{v} - \left(\rho^0 + m_{\mathrm{w}}^+\right)\, \underline{F}_{\mathrm{m}}\cdot\underline{v}\, dx \\ \qquad = \int_{\Gamma_{\mathrm{N}}} \underline{g}_{\mathrm{m,N}}^+ \cdot \mathbf{v}\, dx; \\ \int_\Omega \frac{1}{\Delta t}(m_{\mathrm{w}}^+ - m_{\mathrm{w}}^-)\,\psi + \gamma^+\,(\nabla p_{\mathrm{w}}^+ - \rho_{\mathrm{w}}^+ \underline{F}_{\mathrm{m}})\cdot\nabla\psi\, dx = 0; \\ \int_\Omega \left(\left(\frac{h_{\mathrm{w}}}{\Delta t}(m_{\mathrm{w}}^+ - m_{\mathrm{w}}^-) + \frac{1}{\Delta t}(Q^+ - Q^-) + \gamma^+\,(\nabla p_{\mathrm{w}}^+ - \rho_{\mathrm{w}}^+ \underline{F}_{\mathrm{m}})\cdot\underline{F}_{\mathrm{m}}\right)\, \xi - \left(-h_{\mathrm{w}}^-\,(\nabla p_{\mathrm{w}}^+ - \rho_{\mathrm{w}}^+\underline{F}_{\mathrm{m}}) + \underline{q}\right)\cdot\nabla\xi \right. \\ \qquad = \int_\Omega \Theta^+\, \xi\, dx - \int_{\partial\Omega} g_{\mathrm{t,N}}^+\, \xi\, dx; \end{cases} \tag{31}$$

for all $\underline{v} \in \mathcal{X}^{\mathrm{u}}_{\mathrm{hf}}$ such that $\underline{v} \cdot \underline{n}|_{\partial\Omega\setminus\Gamma_N} = 0$, $\psi \in \mathcal{X}^{\mathrm{p}}_{\mathrm{hf}}$, $\xi \in \mathcal{X}^{\mathrm{t}}_{\mathrm{hf}}$, where

$$\begin{cases} \rho^+_{\mathrm{w}} = \rho^-_{\mathrm{w}} \ \exp\left(\frac{p^+_{\mathrm{w}} - p^-_{\mathrm{w}}}{K_{\mathrm{w}}} \ - \ 3\alpha_{\mathrm{w}}(T^+ - T^-)\right); \\ \varphi^+ = b \ - \ (b - \varphi^-) \ \exp\left(-(\epsilon^+_{\mathrm{V}} - \epsilon^-_{\mathrm{V}}) + 3\alpha_0(T^+ - T^-) \ - \frac{1}{K_s}\ (p^+_{\mathrm{w}} - p^-_{\mathrm{w}})\right); \\ h^+_{\mathrm{w}} = h^-_{\mathrm{w}} + C^{\mathrm{p}}_{\mathrm{w}}\ (T^+ - T^-) + \frac{\beta^{\mathrm{p}}_h - 3\alpha_{\mathrm{w}} T^+}{\rho^+_{\mathrm{w}}}\ \left(p^+_{\mathrm{w}} - p^-_{\mathrm{w}}\right); \\ Q^+ = Q^- + \left(\beta^{\epsilon}_Q + 3\alpha_{\mathrm{s}} K_0\ \frac{1}{2}(T^+ + T^-)\right)\ \left(\epsilon^+_{\mathrm{V}} - \epsilon^-_{\mathrm{V}}\right)\ - \left(\beta^{\mathrm{p}}_Q + 3\alpha^+_{\mathrm{w,m}}\frac{1}{2}(T^+ + T^-)\right)\ \left(p^+_{\mathrm{w}}\ -\ p^-_{\mathrm{w}}\right) \\ \qquad\qquad + C^{0,+}_{\epsilon}\ (T^+ - T^-); \\ m^+_{\mathrm{w}} = \rho^+_{\mathrm{w}}(1 + \epsilon^+_{\mathrm{V}})\ \varphi^+ - \rho^0_{\mathrm{w}}\ \varphi^0. \end{cases} \tag{32}$$

We remark that integrals in system (31)–(32) depend on internal variables at the current times $t^{(j)}$ and at the previous times $t^{(j-1)}$, for $j = 1, \ldots, J_{\max}$: this model problem thus fits in the general problem introduced in Equation (4).

4.4 | Choice of the norm

We equip the FE space $\mathcal{X}_{\mathrm{hf}}$ with the weighted inner product

$$(\underline{U}, \underline{U}') = \frac{1}{\lambda_{\mathrm{u}}}\sum_{d=1}^{2}(\underline{u}_d, \underline{u}'_d)_{H^1(\Omega)} + \frac{1}{\lambda_{\mathrm{p}}}(p, p')_{H^1(\Omega)} + \frac{1}{\lambda_{\mathrm{t}}}(T, T')_{H^1(\Omega)}, \tag{33}$$

where the coefficients λ_{u}, λ_{p}, λ_{t} are the largest eigenvalues of the Gramian matrices $\mathbf{C}^{\mathrm{u}}$, $\mathbf{C}^{\mathrm{p}}$, $\mathbf{C}^{\mathrm{t}}$ associated to displacement, pressure, and temperature, respectively. Similar to Reference 35, the inner product (33) is motivated by the need for properly taking into account the contributions of displacement, pressure, and temperature, which are characterized by different magnitudes and different units.

4.5 | Parameterization

We consider a vector of four parameters: the Young's modulus E and the Poisson's ratio ν in the region UA, the thermic factor τ and the constant C_{al} in (26). For all parameters, we define the parameter domain $\mathcal{P}$ by considering variations of $\pm 15\%$ with respect to the nominal value reported in Table 4.

5 | NUMERICAL RESULTS

We measure performance through the discrete $L^2(0, T_{\mathrm{f}}; \mathcal{X}_{\mathrm{hf}})$ relative error

$$E_\mu := \frac{\sqrt{\sum_{j=1}^{J_{\max}}\left(t^{(j)} - t^{(j-1)}\right)\left\|\underline{U}^{(j)}_{\mathrm{hf},\mu} - \widehat{\underline{U}}^{(j)}_{\mu}\right\|^2}}{\sqrt{\sum_{j=1}^{J_{\max}}\left(t^{(j)} - t^{(j-1)}\right)\|\underline{U}^{(j)}_{\mathrm{hf},\mu}\|^2}} \tag{34}$$

for any $\mu \in \mathcal{P}$. Similarly, we denote by E^{u}_μ, E^{p}_μ, and E^{t}_μ the discrete relative $L^2(0, T_{\mathrm{f}}; \mathcal{X}_{\mathrm{hf}})$ errors associated with the estimate of displacement, pressure, and temperature, respectively.

5.1 | Solution reproduction problem

We first present numerical results for a fixed configuration of parameters $\overline{\mu} \in \mathcal{P}$ to validate the ROM described in Section 3. We consider $\overline{\mu}$ equal to the centroid of $\mathcal{P}$. We perform data compression based on the whole set of snapshots, that is, $|I_{\mathrm{s}}| = J_{\max} = 100$.

5.1.1 | Data compression: POD

In Figure 2, we compare performance of the global POD based on the weighted inner product $(\cdot,\cdot)$ with the performance of the component-wise POD. More precisely, we define $\underline{Z}$ such that

$$[\underline{Z}, \lambda] = \texttt{POD}\left(\{\underline{U}^{(j)}_{\text{hf},\bar{\mu}}\}_{j\in I_s}, (\cdot,\cdot), \text{tol}_{\text{pod}}\right), \tag{35}$$

and we then extract reduced basis associated to the single state variables of interest, that is, we extract the displacement, pressure, and temperature components $\underline{Z}^{\text{u}}, \underline{Z}^{\text{p}}, \underline{Z}^{\text{t}}$.

Then, we denote the "optimal" (in a discrete L^2 sense) spaces

$$[\underline{Z}^{u,\text{opt}}, \lambda^{u,\text{opt}}] = \texttt{POD}\left(\{\underline{u}^{(j)}_{\text{hf},\bar{\mu}}\}_{j\in \mathtt{I}_s}, (\cdot,\cdot)_{H^1}, \text{tol}_{\text{pod}}\right); \tag{36}$$

$$[\underline{Z}^{p,\text{opt}}, \lambda^{p,\text{opt}}] = \texttt{POD}\left(\{p^{(j)}_{\text{hf},\bar{\mu}}\}_{j\in \mathtt{I}_s}, (\cdot,\cdot)_{H^1}, \text{tol}_{\text{pod}}\right); \tag{37}$$

$$[\underline{Z}^{T,\text{opt}}, \lambda^{T,\text{opt}}] = \texttt{POD}\left(\{T^{(j)}_{\text{hf},\bar{\mu}}\}_{j\in \mathtt{I}_s}, (\cdot,\cdot)_{H^1}, \text{tol}_{\text{pod}}\right), \tag{38}$$

that are found through $D_{\text{eq}} - 1$ PODs over displacement, pressure and temperature.

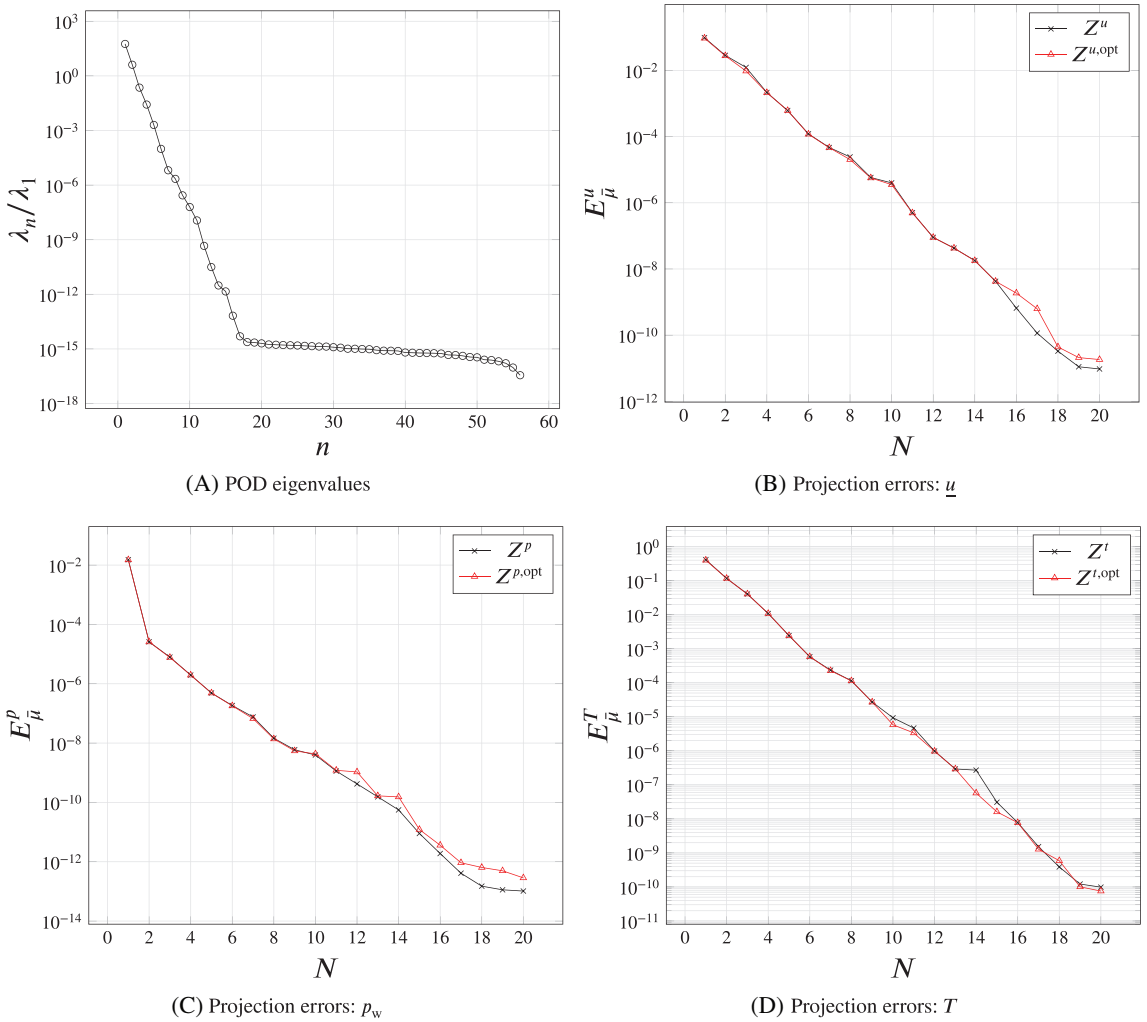

(A) POD eigenvalues (B) Projection errors: $\underline{u}$

(C) Projection errors: p_{w} (D) Projection errors: T

FIGURE 2 Solution reproduction problem. (A) Exponential decay of POD eigenvalues. (B–D) Projection errors computed through (35) (in black) and (36)–(38) (in red) for increasing numbers of POD modes

In Figure 2A, we show the behavior of the POD eigenvalues in (35); in Figure 2B–D, we compare the relative projection errors associated with $\underline{Z}^{u}$ and $\underline{Z}^{u,opt}$, $\underline{Z}^{p}$ and $\underline{Z}^{p,opt}$, and $\underline{Z}^{t}$ and $\underline{Z}^{t,opt}$. We observe that the projection errors are nearly the same for all the three state variables: this observation suggests to consider a single reduced space to approximate the solution field.

5.1.2 | Hyper-reduction

In Figure 3A, we show the performance of the Galerkin ROM with and without hyper-reduction. We distinguish between the high-fidelity quadrature rule, abbreviated as HFQ, and the empirical quadrature rule for several tolerances tol_{eq}. We also add as a reference, the relative projection error. Figure 3B shows the percentage of selected elements $\frac{Q}{N_e} \times 100\%$ for the same choices of the tolerance tol_{eq}. We observe that the empirical quadrature procedure is able to significantly reduce the size of the mesh used for online calculations without compromising accuracy. The plateau for $N \gtrsim 14$ is due to the tolerance of the Newton iterative solver.

In Figure 4, we show the selected grid elements for two choices of the EQ tolerance value tol_{eq} and for $N = 12$. We observe that the sampled elements are distributed over the whole domain with a slight prevalence of elements in the proximity of the alveoli.

We report in Table 5 the computational costs associated to the solution of system (31)–(32) through the high-fidelity solver and the ROM with high-fidelity quadrature and empirical quadrature, for the solution reproduction problem. We consider a reduced space of size $N = 12$; we also set $\text{tol}_{\text{eq}} = 10^{-14}$. The values in Table 5 are the computational speedup, that is, $\text{speedup} = \frac{\text{HF } cost}{\text{ROM } cost}$ where HF *cost* is the computational time of solving the high-fidelity solver and ROM *cost* is the computational time associated to the ROM (we specify in different rows if with HFQ or EQ). The speedup associated to the ROM with high-fidelity quadrature is almost 2 and is more than 50 times lower than the speedup of the hyper-reduced ROM. For this model problem, the cost associated with ROM with HFQ is comparable with the cost of the HF solver. As discussed in Remark 2, the choice of solving a ROM with high-fidelity quadrature significantly increases the offline computation costs.

5.2 | Parametric problem

We present results for the parametric case. We denote by $\Xi_{\text{train}} \subset \mathcal{P}$ the training set used to build the ROM and by $\Xi_{\text{test}} \subset \mathcal{P}$ the test set used to assess performance. Both sets consist of independent identically distributed samples of a uniform

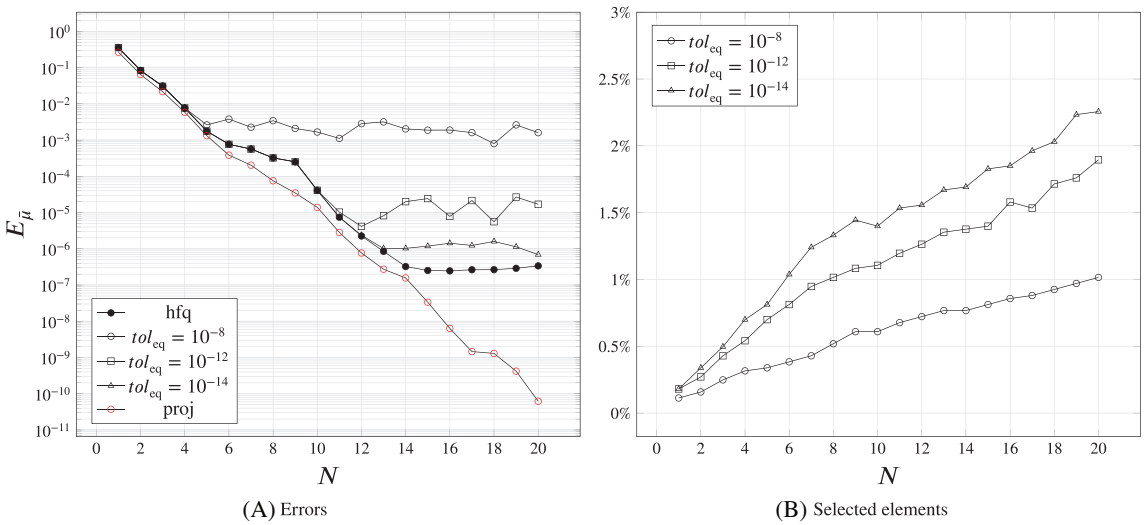

(A) Errors (B) Selected elements

FIGURE 3 solution reproduction problem. (A) Errors associated to projection error (proj), Galerkin with high-fidelity quadrature (HFQ) and Galerkin with empirical quadrature for several choices of tol_{eq} with respect to the ROM dimension N. (B) Percentage of selected elements for several tol_{eq}

distribution in $\mathcal{P}$, with $|\Xi_{\text{train}}| = n_{\text{train}} = 50$ and $|\Xi_{\text{test}}| = n_{\text{test}} = 10$. We also set $\text{tol}_{\text{POD}} = 10^{-7}$ in (8) and in (13b) for data compression, and we set $\text{tol}_{\text{POD,res}} = 10^{-5}$ in (8) for the construction of the empirical test space. We set $I_s \subset \{1, \dots, J_{\max}\}$ with $|I_s| = 20$. EQ rules are depicted using the tolerance $\text{tol}_{\text{eq}} = 10^{-12}$ (cf. Algorithm 4).

5.2.1 | Error estimation

In Figure 5, we compare the dual residual and several EQ errors for each parameter μ in the training set Ξ_{train} and for different dimensions of the reduced space that is progressively updated during the execution of the POD-Greedy algorithm. In particular, we show results in two cases: the hierarchical POD-Greedy (H-POD) and the hierarchical approximate POD-Greedy (denoted as HA-POD). Figure 5A,B shows for both H-POD and HA-POD to what extent the residual-based error indicator defined in (17) is correlated with the relative error (34). We observe that for values of the indicators that are larger than 10^{-3}, correlation is very high, while for smaller values correlation is much weaker.

To provide a concrete reference, in Figure 6, we investigate the correlation between the relative error (34) and the time-discrete $L^2(0, T_f; \mathcal{X}'_{\text{hf},0})$ residual indicator defined in (21): we observe that the indicator in (21) is significantly more accurate, particularly for small values of the error. As stated in Section 3, the residual indicator (21) is considerably more expensive in terms of both memory and computational costs.

5.2.2 | POD-Greedy sampling

In Figures 7 and 8, we show the POD-Greedy algorithm convergence history, for both the hierarchical and approximate hierarchical PODs. At each iteration of the algorithm, until convergence, the error indicator Δ_μ is illustrated with respect to training parameter indices $\mathcal{I}_{\text{train}} = \{1, \dots, |\Xi_{\text{train}}|\}$. At each iteration the selected parameter $\mu^\star$ is marked in red, while

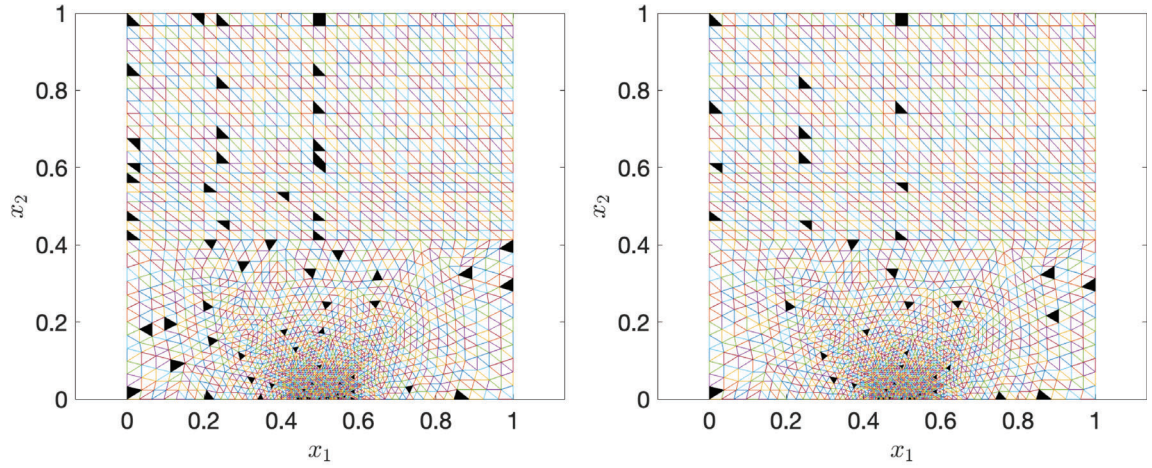

(A) $tol_{\text{eq}} = 10^{-14}$ (B) $tol_{\text{eq}} = 10^{-10}$

FIGURE 4 solution reproduction problem. Reduced mesh for two choices of the empirical quadrature tolerance

TABLE 5 Solution reproduction problem: Relative computational costs of the ROM with high-fidelity quadrature and empirical quadrature

	Speedup
HF	1
ROM with HFQ	1.87
ROM with EQ	104.60

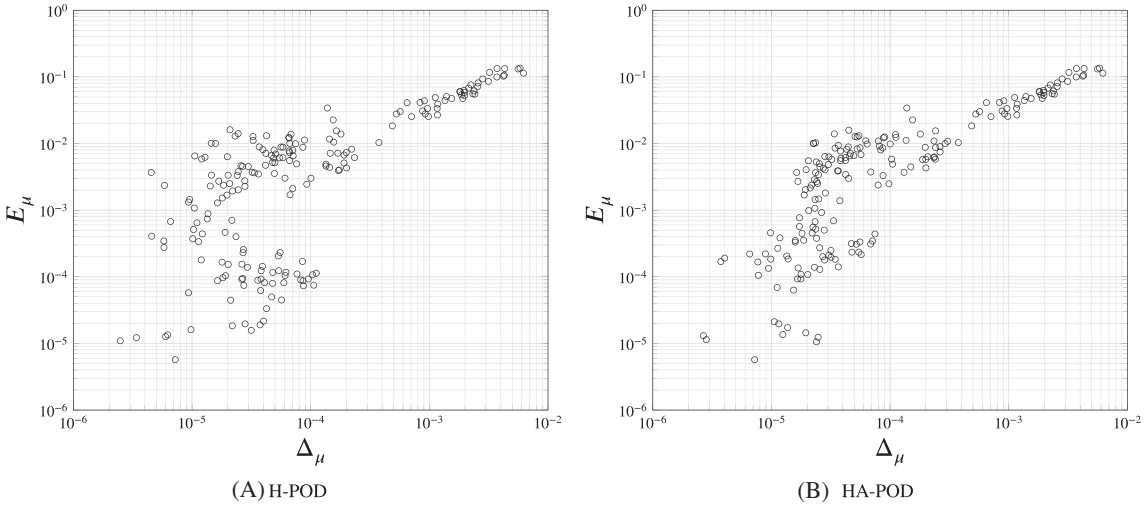

FIGURE 5 Parametric problem: Correlation between the time-average residual indicator (17) and true relative errors (34)

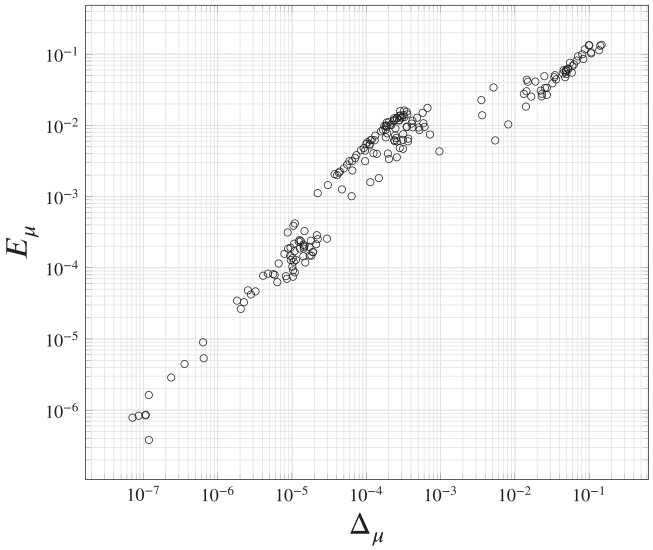

FIGURE 6 Parametric problem: Correlation between residual indicator (21) and true relative errors (34)

the previously selected parameters are marked in green. We also report the dimension of the updated reduced space and the number of sampled elements.

5.2.3 | Prediction tests

In Figure 9, we assess out-of-sample performance of the proposed method. More precisely, we show the behavior of the maximum relative error (34) over the test set $\max_{\mu\in\Xi_{\text{test}}} E_\mu$ for both H-POD Greedy and HA-POD Greedy. To provide a relevant benchmark, we compare results with the H-POD Greedy and HA-POD Greedy algorithms based on the exact errors (strong POD-Greedy). For this particular example, we observe that the proposed method is effective to generate accurate ROMs: in particular, the Greedy procedures based on the time-averaged error indicator are comparable in terms of performance with the corresponding strong POD-Greedy algorithms.

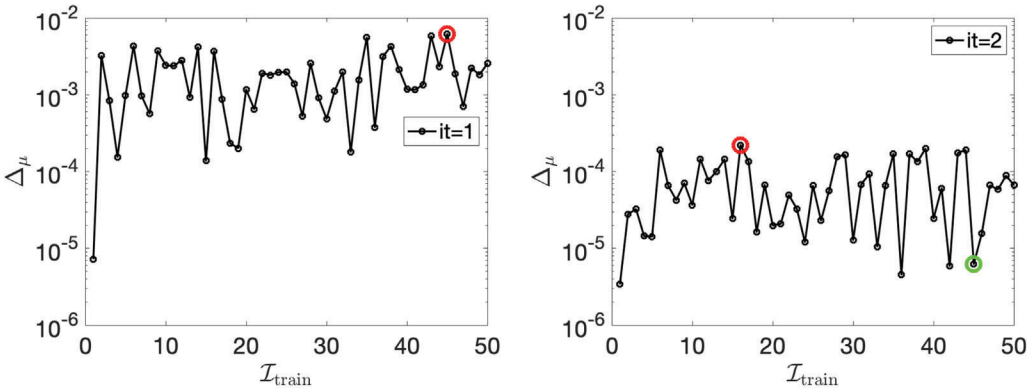

(A) Iteration it = 1; $N = 15$, $Q = 74$, $Q_r = 16$ (B) Iteration it = 2; $N = 26$, $Q = 123$, $Q_r = 18$

(C) Iteration it = 3; $N = 35$, $Q = 155$, $Q_r = 22$ (D) Iteration it = 4; $N = 43$, $Q = 169$, $Q_r = 18$

FIGURE 7 Parametric problem: POD-Greedy algorithm convergence history in the H-POD case

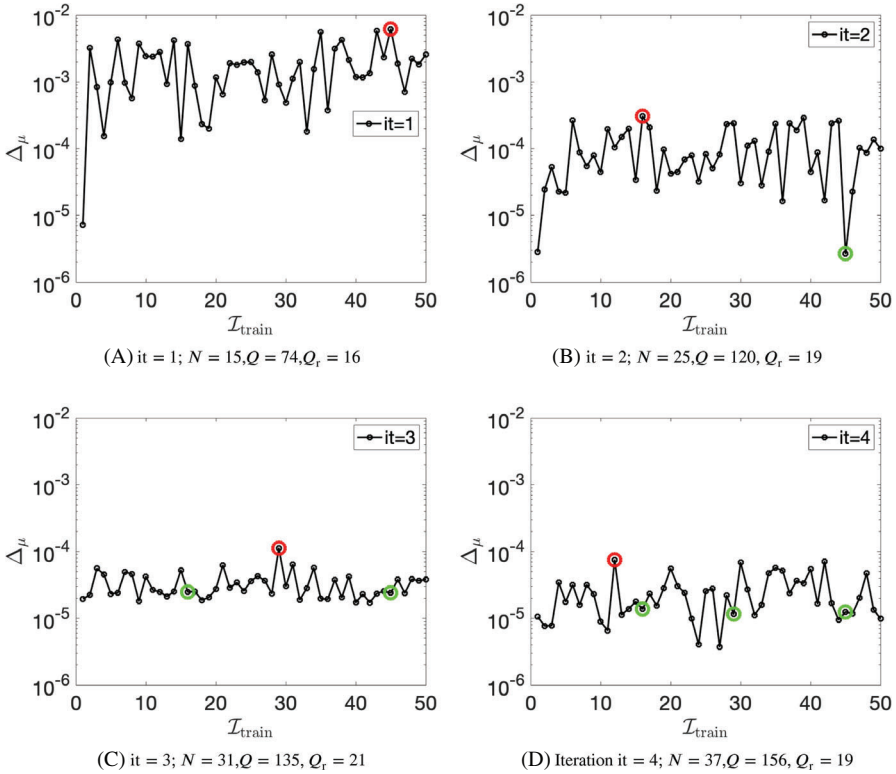

(A) it = 1; $N = 15$,$Q = 74$,$Q_r = 16$ (B) it = 2; $N = 25$,$Q = 120$, $Q_r = 19$

(C) it = 3; $N = 31$,$Q = 135$, $Q_r = 21$ (D) Iteration it = 4; $N = 37$,$Q = 156$, $Q_r = 19$

FIGURE 8 Parametric problem: POD-Greedy algorithm convergence history in the HA-POD case

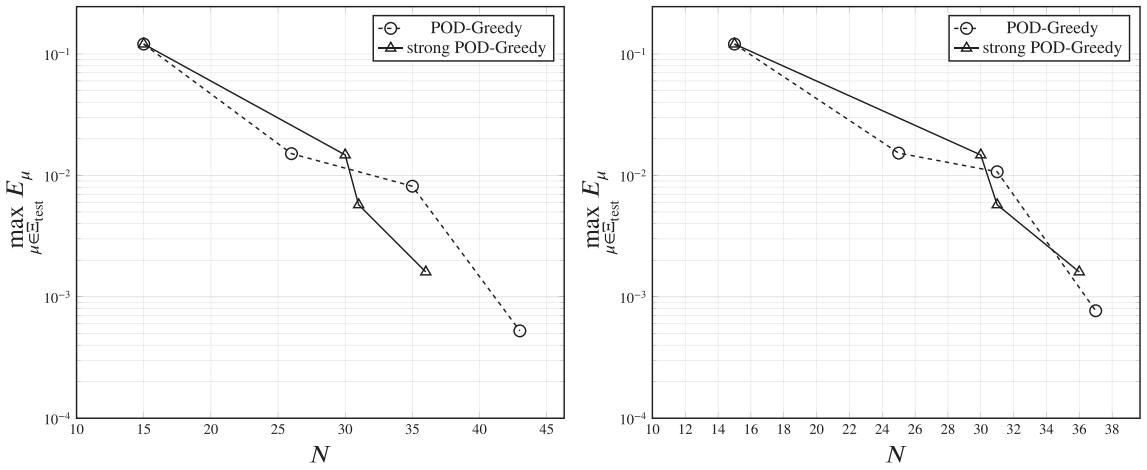

(A) H-POD Greedy (B) HA-POD Greedy

FIGURE 9 Parametric problem: Out-of-sample performance of the ROM parametric problem obtained using the POD-Greedy algorithm. Comparison with strong POD Greedy

6 | CONCLUSIONS

In this work, we developed and numerically validated an MOR procedure for a class of problems in nonlinear mechanics, and we successfully applied it to a two-dimensional parametric THM problem that arises in radioactive waste management. We proposed a time-averaged error indicator to drive the offline Greedy sampling, and an empirical quadrature procedure to reduce offline costs.

We aim to extend the approach in several directions. First, we wish to apply our method to other problems of the form (1), to demonstrate the generality of the approach and its relevance for continuum mechanics applications. Second, we wish to combine our approach with domain decomposition methods[36-38] to deal with more complex parameterizations and topological changes. Toward this end, we wish to devise effective localized training methods to reduce offline costs and domain decomposition strategies to glue together the solution in different components of the domain.

ACKNOWLEDGMENTS

The authors acknowledge the financial support of Andra (National Agency for Radioactive Waste Management) and thank Dr. Marc Leconte and Dr. Antoine Pasteau (Andra) for fruitful discussions. The authors also acknowledge the support by European Union's Horizon 2020 Research and Innovation Programme under the Marie Sk lodowska-Curie Actions, grant agreement 872442 (ARIA).

CONFLICT OF INTEREST

The authors declare no potential conflict of interests.

DATA AVAILABILITY STATEMENT

The data used to support the findings of this work are included within the article. In particular, physical parameters of the THM model can be found in Table 4 (we suggest to see also Reference 39). Raw numerical data that have been used to generate tables and figures in the paper as well as the Matlab source files are available upon request.

ORCID

Giulia Sambataro https://orcid.org/0000-0003-2518-1525

REFERENCES

1. Hesthaven JS, Rozza G, Stamm B. *Certified Reduced Basis Methods for Parametrized Partial Differential Equations*. Springer; 2016.
2. Quarteroni A, Manzoni A, Negri F. *Reduced Basis Methods for Partial Differential Equations: An Introduction*. Vol 92. Springer; 2015.
3. Rozza G, Huynh DBP, Patera AT. Reduced basis approximation and a posteriori error estimation for affinely parametrized elliptic coercive partial differential equations. *Arch Comput Methods Eng*. 2007;15(3):229-275.

4. Farhat C, Chapman T, Avery P. Structure-preserving, stability, and accuracy properties of the energy-conserving sampling and weighting method for the hyper reduction of nonlinear finite element dynamic models. *Int J Numer Methods Eng*. 2015;102(5):1077-1110.
5. Yano M. Discontinuous Galerkin reduced basis empirical quadrature procedure for model reduction of parametrized nonlinear conservation laws. *Adv Comput Math*. 2019;45:2287-2320.
6. Yano M, Patera AT. An LP empirical quadrature procedure for reduced basis treatment of parametrized nonlinear PDEs. *Comput Methods Appl Mech Eng*. 2019;344:1104-1123.
7. Riffaud S, Bergmann M, Farhat C, Grimberg S, Iollo A. The DGDD method for reduced-order modeling of conservation laws. *J Comput Phys*. 2021;437:110336.
8. Taddei T, Zhang L. A discretize-then-map approach for the treatment of parameterized geometries in model order reduction. *Comput Methods Appl Mech Eng*. 2021;384:113956.
9. Farhat C, Avery P, Chapman T, Cortial J. Dimensional reduction of nonlinear finite element dynamic models with finite rotations and energy-based mesh sampling and weighting for computational efficiency. *Int J Numer Methods Eng*. 2014;98(9):625-662.
10. Zahr M, Avery P, Farhat C. A multilevel projection-based model order reduction framework for nonlinear dynamic multiscale problems in structural and solid mechanics. *Int J Numer Methods Eng*. 2017;112(8):855-881.
11. Barrault M, Maday Y, Nguyen NC, Patera AT. An empirical interpolation method: application to efficient reduced-basis discretization of partial differential equations. *C R Math*. 2004;339(9):667-672.
12. Chaturantabut S, Sorensen DC. Nonlinear model reduction via discrete empirical interpolation. *SIAM J Sci Comput*. 2010;32(5):2737-2764.
13. Ryckelynck D. Hyper-reduction of mechanical models involving internal variables. *Int J Numer Methods Eng*. 2009;77(1):75-89.
14. Carlberg K, Farhat C, Cortial J, Amsallem D. The GNAT method for nonlinear model reduction: effective implementation and application to computational fluid dynamics and turbulent flows. *J Comput Phys*. 2013;242:623-647.
15. Willcox K. Unsteady flow sensing and estimation via the gappy proper orthogonal decomposition. *Comput Fluids*. 2006;35(2):208-226.
16. Casenave F, Akkari N, Bordeu F, Rey C, Ryckelynck D. A nonintrusive distributed reduced-order modeling framework for nonlinear structural mechanics-Application to elastoviscoplastic computations. *Int J Numer Methods Eng*. 2018;121(1):32-53.
17. Hernández J, Caicedo M, Ferrer A. Dimensional hyper-reduction of nonlinear finite element models via empirical cubature. *Comput Methods Appl Mech Eng*. 2017;313:687-722.
18. Haasdonk B, Ohlberger M. Reduced basis method for finite volume approximations of parametrized linear evolution equations. *ESAIM Math Model Numer Anal*. 2008;42(2):277-302.
19. Haasdonk B. Convergence rates of the POD-greedy method. *ESAIM Math Model Numer Anal*. 2013;47(3):859-873.
20. Berkooz G, Holmes P, Lumley J. The proper orthogonal decomposition in the analysis of turbulent flows. *Annu Rev Fluid Mech*. 1993;25(1):539-575.
21. Bergmann M, Bruneau CH, Iollo A. Enablers for robust POD models. *J Comput Phys*. 2009;228(2):516-538.
22. Volkwein S. *Model Reduction Using Proper Orthogonal Decomposition. Lecture Notes*. Institute of Mathematics and Scientific Computing, University of Graz. www.math.uni-konstanz.de/numerik/personen/volkwein/teaching/POD-Vorlesung.pdf; 2011:1025.
23. Fick L, Maday Y, Patera AT, Taddei T. A stabilized POD model for turbulent flows over a range of Reynolds numbers: optimal parameter sampling and constrained projection. *J Comput Phys*. 2018;371:214-243. doi:10.1016/j.jcp.2018.05.027
24. Miled B, Ryckelynck D, Cantournet S. A priori hyper-reduction method for coupled viscoelastic–Viscoplastic composites. *Comput Struct*. 2013;119:95-103.
25. Leuschner M, Fritzen F. Reduced order homogenization for viscoplastic composite materials including dissipative imperfect interfaces. *Mech Mater*. 2017;104:121-138.
26. Larion Y, Zlotnik S, Massart TJ, Díez P. Building a certified reduced basis for coupled thermo-hydro-mechanical systems with goal-oriented error estimation. *Comput Mech*. 2020;66(3):559-573.
27. Granet S. Modélisations THHM. Généralités et algorithmes; 2009. https://www.code-aster.org/V2/doc/v9/fr/man_r/r7/r7.01.10.pdf
28. Sirovich L. Turbulence and the dynamics of coherent structures. I. Coherent structures. *Q Appl Math*. 1987;45(3):561-571.
29. Slawski M, Hein M. Sparse recovery by thresholded non-negative least squares. 24th International conference of neural information processing system of December. 2011:1926-1934.
30. Lawson CL, Hanson RJ. *Solving Least Squares Problems*. Vol 161. SIAM; 1974.
31. Chapman T, Avery P, Collins P, Farhat C. Accelerated mesh sampling for the hyper reduction of nonlinear computational models. *Int J Numer Methods Eng*. 2017;109(12):1623-1654.
32. Haasdonk B. Reduced basis methods for parametrized PDEs–a tutorial introduction for stationary and instationary problems. *Model Reduct Approx Theory Algorithms*. 2017;15:65.
33. Himpe C, Leibner T, Rave S. Hierarchical approximate proper orthogonal decomposition. *SIAM J Sci Comput*. 2018;40(5):A3267-A3292.
34. Brand M. Fast online SVD revisions for lightweight recommender systems. Proceedings of the 2003 SIAM International Conference on Data Mining; 2003:37-46; SIAM.
35. Taddei T. An offline/online procedure for dual norm calculations of parameterized functionals: empirical quadrature and empirical test spaces. *Adv Comput Math*. 2019;45(5–6):2429-2462.
36. Bergmann M, Ferrero A, Iollo A, Lombardi E, Scardigli A, Telib H. A zonal Galerkin-free POD model for incompressible flows. *J Comput Phys*. 2018;352:301-325.

37. Kaulmann S, Ohlberger M, Haasdonk B. A new local reduced basis discontinuous Galerkin approach for heterogeneous multiscale problems. *C R Math*. 2011;349(23-24):1233-1238.
38. Huynh DBP, Knezevic DJ, Patera AT. A static condensation reduced basis element method: approximation and a posteriori error estimation. *ESAIM Math Model Numer Anal*. 2013;47(1):213-251.
39. Granet S. Modélisations thhm généralités et algorithmes. *Document Aster*. 2009;R7(1):1-32.

How to cite this article: Iollo A, Sambataro G, Taddei T. An adaptive projection-based model reduction method for nonlinear mechanics with internal variables: Application to thermo-hydro-mechanical systems. *Int J Numer Methods Eng*. 2022;123(12):2894-2918. doi: 10.1002/nme.6964